修士論文

単層カーボンナノチューブの直径制御 CVD 合成

Diameter controlled CVD growth of single-walled carbon nanotubes

1 - 58 ページ 完

平成 22 年 8 月 20 日提出

Submitted on Aug. 20, 2010

指導教員 丸山茂夫教授

Supervised by Professor Shigeo Maruyama

Theerapol THURAKITSEREE

37-085938 トゥラキットセーリー　ティーラポン

Contents

Chapter 1

Introduction

1.1 Organization

This thesis begins with a brief introduction to SWNTs, followed by a discussion of some of the physical properties of SWNTs. This will provide the foundation upon which the results presented later will be based. After the general introduction, a few general techniques for characterizing and evaluating SWNTs are introduced, which will be referenced throughout this work. The history of SWNTs synthesis will be reviewed, and several methods will be presented for diameter control.

The results of the research conducted during the Master course are presented starting from Chapter 4, which discusses the investigation of diameter control of SWNTs. In this study, several methods were investigated to control the diameter of SWNT. The studied topics were influenced by many parameters, which affected the diameter such as ambient gas, supporting substrate, catalysts pre-treatment, catalyst recipe, and the catalyst itself. The influence of those parameters and the controlled diameter of SWNTs were lastly presented through optical methods. In addition, a new noble metal was also presented as a catalyst for SWNT growth.

SWNTs represent one form of carbon material, which is a one the most wondrous materials in the world with a one-dimensional (1D) cylindrical structure that is formed by rolling of a graphene sheet (2D). After the discovery of a new allotrope of carbon which is called fullerene (0D) in 1985 by Robert F. Curl, Sir Harold W. Kroto, and Richard E. Smalley [1], 1D carbon with a tubular structure had been imagined. In 1993, this kind of this structure called SWNTs was successful discovered by Iijima and Ichihashi [2]. After this step, there were a lot of reports and experimental studies on SWNTs in order to achieve this structure more productively, such as laser furnace (1996) [3], arc-discharge

(1997) [4], chemical vapour deposition (CVD) with supported catalysts (1996) [5] and floated catalysts (1998) [6,7]. Although, these methods are good for mass synthesis of SWNT, purification processes are required. At the same time, the CVD technique with supported catalysts became more interesting. The ACCVD process [8] has been developed and can produce high yield with a high quality. SWNT is emphasized more and more because of its outstanding mechanical and electronic property, etc. They are dependent on their geometric structure called chirality [9]; more details of SWNT would be discussed in the next section. Most the material in this chapter can be found in comprehensive texts such as Ref [9,29].

1.2 Fundamental and structure representation of SWNT

An SWNT is defined as a cylindrical graphene sheet with a diameter of about 0.7-10.0 nm. Since the length is much larger compared to its diameter, SWNT can be though as a one-dimensional (1D) nanostructure. Interestingly, the electronic structure of SWNT is has determined the orientation of the six-member carbon ring in the honeycomb lattice relative to the axis of the nanotube is called a hexagon. A SWNT can be described as a graphene sheet rolled into a cylindrical shape, which is a one-dimensional structure with axial symmetry, and different structures and properties depended upon the rolling direction, called chirality that exhibit spiral conformation. Figure 1-1 shows three samples of SWNTs rolled in three different directions. Furthermore, the electronic structure of SWNT can be either metallic or semiconducting, depending on its diameter and chirality.

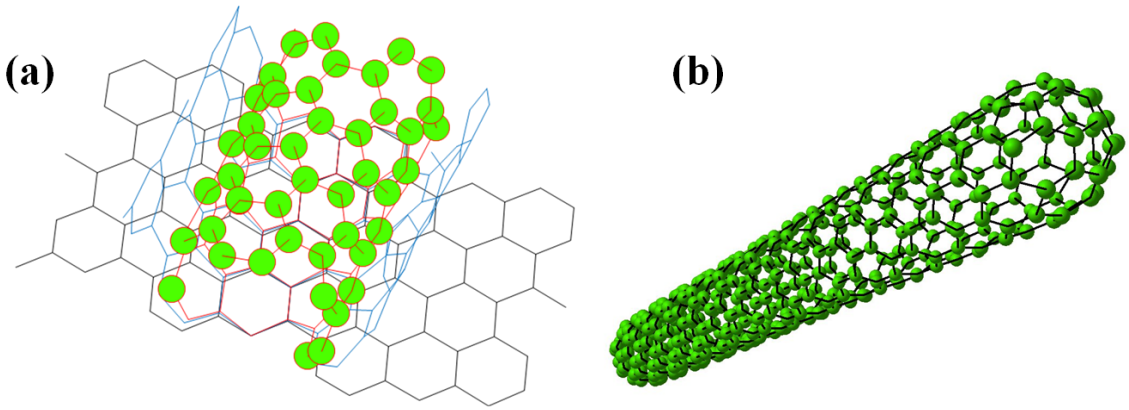

Figure 1-1 (a) Graphene is rolled up into a tube, and (b) an example of SWNTs.

The Structure and electronic property of a single-walled carbon nanotube

As mentioned before, the structure of an SWNT is based on the two-dimensional (2D) graphene sheet. To describe the geometry of SWNT, it can be described from graphene structure. The structure of a 2D graphene is the hexagonal like structure shown in Figure 1-2 that has a unit cell of hexagonal lattice containing two-equivalent C atoms with the distance between neighbouring atoms a_{C-C} 1.42 Å. Vectors $\boldsymbol{a}_1$ and $\boldsymbol{a}_2$ are represented as the unit vectors of the cell. Based on Cartesian coordinates, these unit vectors can be written by

$$\boldsymbol{a}_1 = \left(\frac{\sqrt{3}a}{2}, \frac{a}{2}\right) \quad \boldsymbol{a}_2 = \left(\frac{\sqrt{3}a}{2}, -\frac{a}{2}\right)$$

where the lattice constant is defined as the magnitude of the vector $\boldsymbol{a}_1$ or $\boldsymbol{a}_2$ that is $a \equiv |\boldsymbol{a}_1| = |\boldsymbol{a}_2| = 1.42\ \text{Å} \times \sqrt{3} = 2.46\ \text{Å}$, while vectors $\boldsymbol{b}_1$ and $\boldsymbol{b}_2$ are the reciprocal vectors in the Brillouin zone (BZ) of the graphene as the shadowed hexagon (Figure 1-2), written in k_x-k_y coordinates as expressed by

$$\boldsymbol{b}_1 = \left(\frac{2\pi}{\sqrt{3}a}, \frac{2\pi}{a}\right) \quad \boldsymbol{b}_1 = \left(\frac{2\pi}{\sqrt{3}a}, \frac{2\pi}{a}\right)$$

Since the structure of the SWNT is formed from a rolled graphene sheet, unrolled hexagonal lattice of a SWNT is modified, and the unit cell of SWNT is enlarged when compared to that of the graphene due to the lower symmetry of SWNTs. There are two vectors to describe the geometry of a SWNT. As shown in Figure 1-3, $\boldsymbol{C}_h$ called the chiral vector for the rolling direction and the translational vector ($\boldsymbol{T}$) for the direction of the SWNT axis. These vectors connect two crystallographically equivalent sites in the

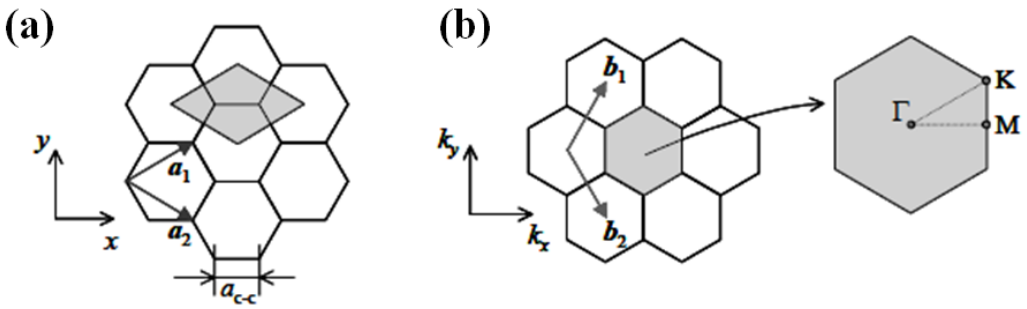

Figure 1-2 (a) The unit cell and (b) Brillouin zone of graphene (enclosed by the shadowed rhombus and hexagon, respectively, and the high-symmetric points in the 2D Brillouin zone conventionally called Γ, K, and M point. The unit vectors and reciprocal lattice vectors are represented by a_i and b_i $(i = 1, 2)$, respectively.

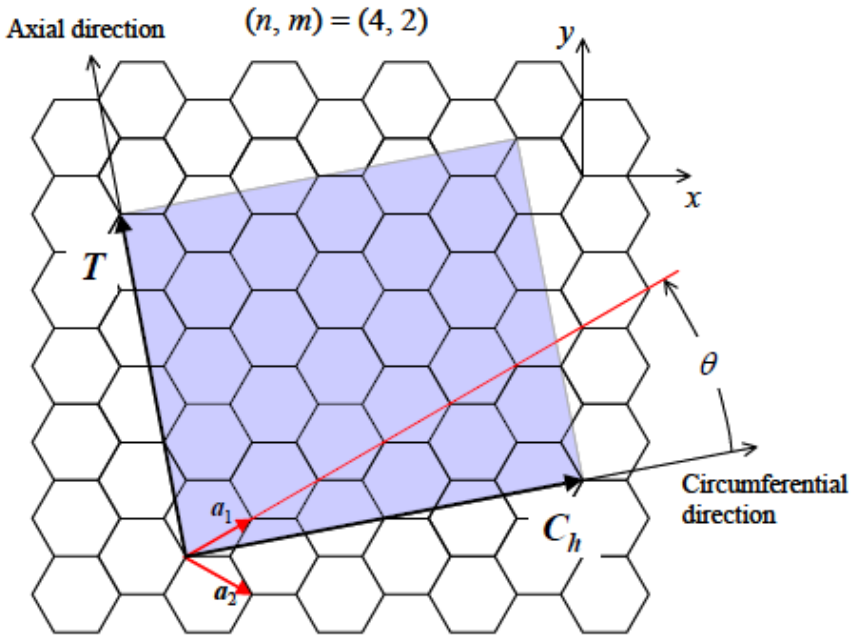

Figure 1-3 the chiral vector $\boldsymbol{C}_h$ for an $(n,m) = (4,2)$ SWNT, containing 28 hexagons in unit cell denoted as shadowed area. The chiral angle is shown by θ.

circumferential and axial directions of the SWNT, respectively, where the unit cell of a certain type of SWNT is indicated as a shadowed area.

The chiral vector $\boldsymbol{C}_h$ is expressed in terms of real-space unit vectors $\boldsymbol{a}_1$ or $\boldsymbol{a}_2$ and two integers n and m $(0 \leq m \leq n)$ as $\boldsymbol{C}_h = n\boldsymbol{a}_1 + m\boldsymbol{a}_2 \equiv (n,m)$. Since the length of $\boldsymbol{C}_h$ indicates the circumferential length of the SWNT, the diameter of the SWNT (d_t) is expressed as

$$d_t = \frac{|\boldsymbol{C}_h|}{\pi} = \frac{\sqrt{\boldsymbol{C}_h . \boldsymbol{C}_h}}{\pi} = \frac{a\sqrt{n^2 + m^2 + nm}}{\pi}$$

As for the chiral angle θ, due to the hexagonal symmetry of the honeycomb lattice, the angle formed by $\boldsymbol{C}_h$ and $\boldsymbol{a}_1$ can be written in terms of the chiral vector θ $(0 \leq \theta \leq 30^{\circ})$ that is expressed as

$$\cos\theta = \frac{\boldsymbol{C}_h . \boldsymbol{a}_1}{|\boldsymbol{C}_h| . |\boldsymbol{a}_1|} = \frac{2n + m}{2\sqrt{n^2 + m^2 + nm}}$$

In the SWNT's direction, which is the direction of the translational vector $\boldsymbol{T}$ parallel to the SWNT axis and perpendicular to $\boldsymbol{C}_h$, this vector $\boldsymbol{T}$ is defined as the unit vector of a 1D SWNT. From the relationship $\boldsymbol{C}_h . \boldsymbol{T} = 0$, we can get

$$\boldsymbol{T} = t_1\boldsymbol{a}_1 + t_2\boldsymbol{a}_2 \equiv (t_1, t_2), \quad t_1 = \frac{2m+n}{d_R}, \quad t_2 = -\frac{2n+m}{d_R}$$

where d_R is the greatest common divisor (gcd) of $(2m+n)$ and $(2n+m)$. By introducing d as the gcd of n and m, d_R can be written based on Euclid's law [1] by

$$d_R = \begin{cases} d \text{ if } n-m \text{ is not a multiple of } 3d \\ 3d \text{ if } n-m \text{ is a multiple of } 3d. \end{cases}$$

When the area of the shadowed rectangular is divided by the area of the hexagon, the number of hexagons in the unit cell of a SWNT N is expressed as

$$N = \frac{|\boldsymbol{C}_h \times \boldsymbol{T}|}{|\boldsymbol{a}_1 \times \boldsymbol{a}_2|} = \frac{2(n^2+m^2+nm)}{d_R}$$

Using the definition of the structure of SWNT, the electronic structure of a SWNT can be obtained by a tight-binding calculation from 2D graphite. Because the SWNT is a 1D tube and has the vector $\boldsymbol{C}_h$ and $\boldsymbol{T}$ in the rolling and axis directions, its energy band gap can be considered from the energy dispersion relations of a 2D graphene. When the energy dispersion relation of 2D graphene is denoted as $E_{g,2D}(k)$, thus N pairs of 1D energy dispersion relation $E_\mu(k)$ can be expressed as

$$E_\mu(k) = E_{g,2D}\left(k\frac{\boldsymbol{K}_2}{|\boldsymbol{K}_2|} + \mu\boldsymbol{K}_1\right), \quad (\mu = 0, \dots, N-1, \text{and} -\frac{\pi}{|\boldsymbol{T}|} < k < \frac{\pi}{|\boldsymbol{T}|})$$

where k denotes the wave number along the SWNT axis. If these energy dispersion curves are collected (or folded) into the first Brillouin zone of the 2D graphene by translating them, using multiples of $\boldsymbol{K}_1$ and$\boldsymbol{K}_2$, we would obtain what is shown in Figure 1-4. The wave vectors possible in the case of an SWNTs are limited from the case of 2D graphene. If the cutting line (along vector $\boldsymbol{K}_2$) passes through the $\boldsymbol{K}$ point, the 1D energy bands will have zero energy gaps and the density of state at Fermi energy levels will have a finite value, then that SWNT will be metallic. On the other hand, it will be semiconducting in the case of non-zero energy gaps when the cutting line does not pass through the $\boldsymbol{K}$ point. The formation of discrete bands is a result of the periodic boundary condition around the circumference direction of the SWNT. Van Hove singularities are present in the resulting electronic density of state (Fig. 1-5). Since the (4,2) SWNT is an intrinsic semiconductor, the density of state at Fermi level is zero. On the other hand, the density of state for the (6,6) SWNT is more than zero because it is inherently metallic.

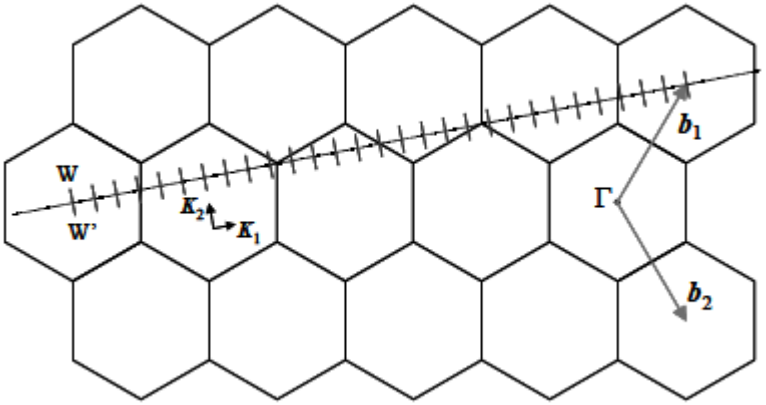

Figure 1-4 Cutting lines in the Brillouin zone for a (4,2) nanotube.

Therefore, one of the most important characteristics of SWNTs is that the difference of metallic/semiconducting transport properties is determined by the chirality. Figure 1-6 shows the chiral mapping of (n, m) SWNTs that are either metallic (black dots) or semiconducting (red dots). Any chirality is specified either by two integers (n, m) or equivalently. Among these, the SWNTs with $m = 0$ (i.e., $\theta = 0°$) and $n = m$ (i.e., $\theta = 30°$) chirality are termed "*zig-zag*" and "*armchair*" types, respectively. This is because of their shapes at the edges that look like a zigzag and an armchair, but there is one type of SWNT which does not belong to both types that are called "*chiral*" type, as shown in Fig. 1-7. In addition, there is one principle that is used to identify which SWNTs are metallic or semiconducting SWNT. The SWNTs are metallic if $\mathrm{mod}(n - m, 3) = 0$, whereas they are semiconducting if $\mathrm{mod}(n - m, 3) \neq 0$. This characteristic is also shown in chirality mapping.

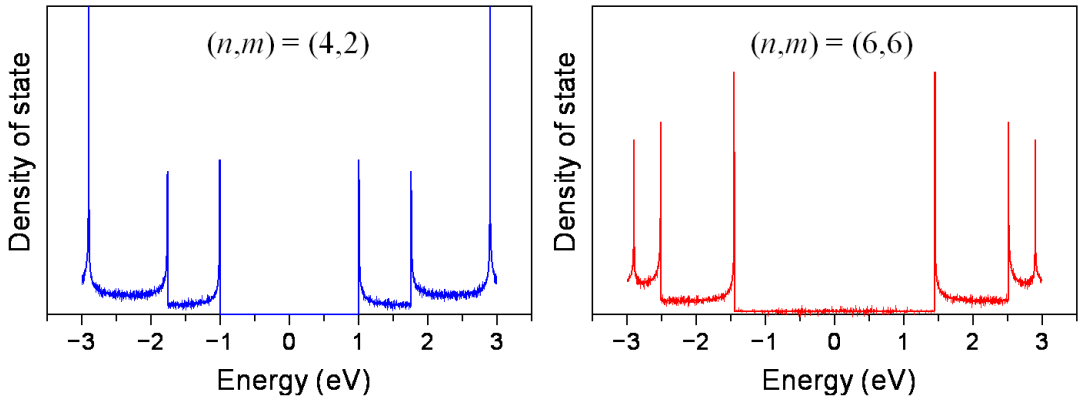

Figure 1-5 Plots of the density of states for a semiconducting (4,2) chiral SWNT, and a metallic (6,6) armchair SWNT.

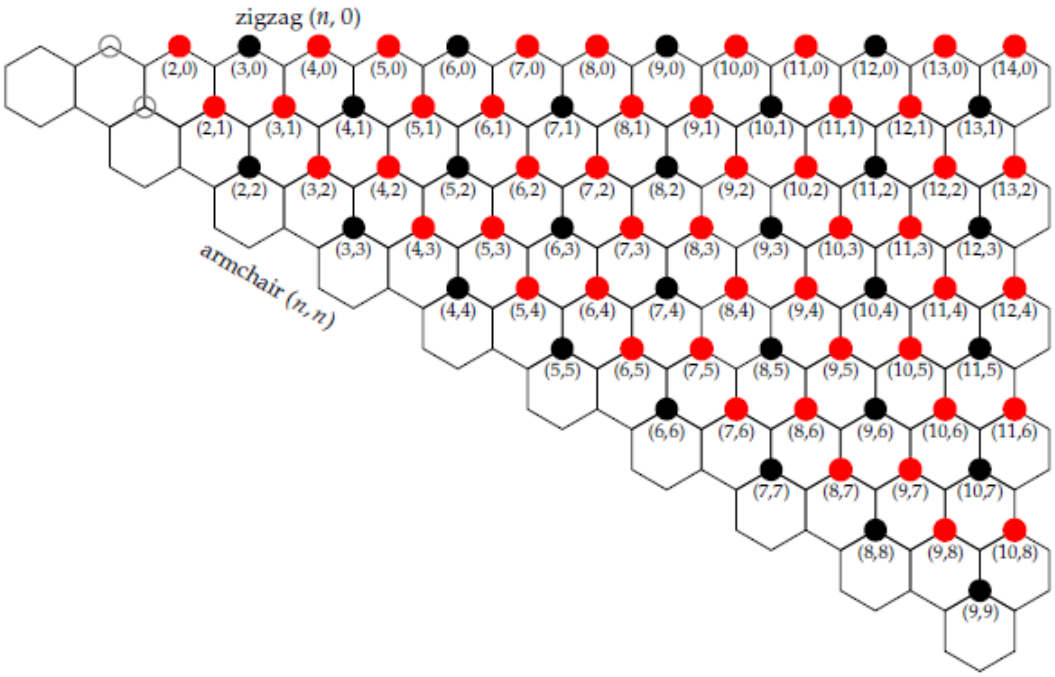

Figure 1-6 Representation of the symmetry-dependent electrical properties of SWNTs, where each dot corresponds to a specific chirality. The red dots represent semiconducting nanotubes, while the black dots are for metallic nanotubes.

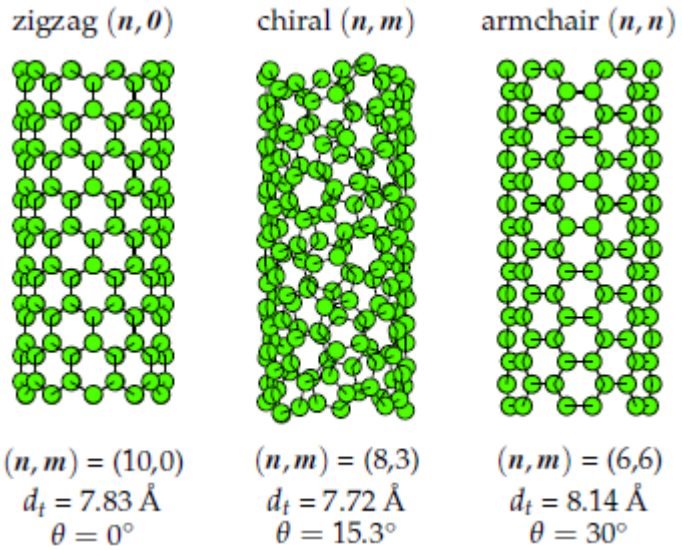

Figure 1-7 Structure of zig-zag, armchair, and chiral type SWNTs represented by $(n, m) = (10,0), (8,8)$ and $(10,5)$ tubes, respectively.

Chapter 2

Characterization methods

Since the properties of SWNTs are depended upon the electronic structure of SWNTs, called chiralities (*n*,*m*), the control of the diameter of SWNT is a promising control structure of the SWNTs because the number of chiralities will be small with narrow in diameter distributions, so for that purpose in this chapter many methods will be presented to control the diameter of SWNTS. In the previous section some fundamentals of SWNTs were discussed. The electrical property of SWNTS is controlled by the electronic density of state, and depends on the (*n*,*m*) chirality structure. To get information on the electronic structure and diameter, optical techniques were used to characterize SWNTs, which are commonly used in the nanotube research field. Furthermore, electron microscopes are also employed to reveal the morphologies and structures of as-grown SWNTs. Even though electron microscopy sometime cannot give enough information such as, diameter and impurity, it can be used to see a larger area of samples than the optical tools, where only small amounts or areas of samples can be seen.

2.1 Resonance Raman spectroscopy

2.1.1 Nature of Raman scattering

Resonance Raman spectroscopy is one of easies and quick characterizing tools, which can give a lot of information about the presence, structure and properties of SWNT, impurity, and also roughly identifying the diameter and its structure for SWNT. The principle of the resonance Raman spectroscopy is expressed by the inelastic scattering of e photon, which is related to the phenomenon of the change in frequency when light is scattered by molecules. The presence of scattered lines of shifted frequencies can be

understood by considering the incident light to consist of photons of energy. For the collision with a molecule, a photon may be elastically scattered without change of energy which gives rise to the Rayleigh line and this is how most scattering events of the process take place. However, the collision may be inelastic, they may cause the molecule to get a quantum transition to a higher energy level, which would make the photon lose energy and thus is scattered with a lower frequency. If the molecule is already at an energy level above its lowest, an encounter with a photon may cause it to undergo a transition to a lower energy, which the photon is scattered with increased frequency. Thus, we can see that the Raman shifts are equivalent to the energy changes involved in transitions of the scattering species. In fact, Raman shifts correspond to vibrational or rotational transitions of the scattering molecules, but the photon is never absorbed, just rather perturbs the molecule and induces it to undergo this phenomenon.

If we consider the energy level of the scattering molecule by the incident light with a frequency υ_0, when the energy of the level m (E_m) and n are equivalent (E_n) ($h\upsilon=0$) as shown in Figure 2-1, the state of the scattering molecule remains unchanged and we can get the Rayleigh scattering. In the case of similar energy levels, if they are not the same, the Raman effect will occur, however if the transition is induced to a lower energy ($E_m > E_n$), that state if its energy will be negative, is called ani-Stoke Raman line. Vice versa, it is called a Stokes line (positive) if the state of energy is upped to higher energy or positive ($E_m < E_n$). Therefore, it can be noted that the Raman scattering is incoherent and Rayleigh scattering is coherent. The events of scattering can be simply explained by the following example: (1) electron is excited from the valence band to conduction band by absorbing a

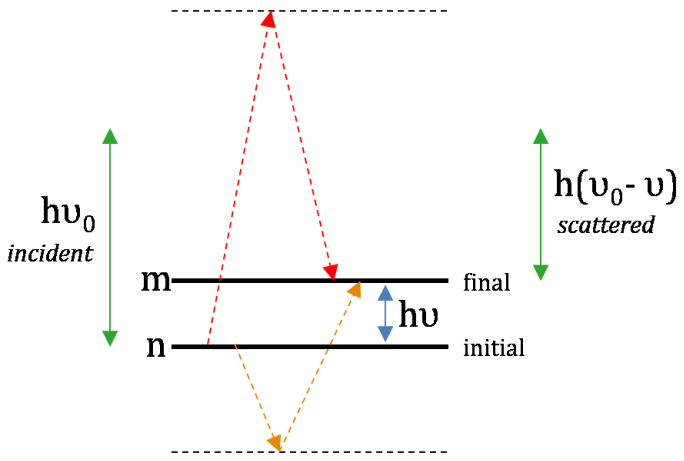

Figure 2-1 Excitation of a Stokes Raman line (H. A. Szymanski, *Raman spectroscopy: Theory and practice*, Plenum press, New York, (1967), p. 9).

photon, (2) the excited electron is scattered by emitting or absorbing phonons, and (3) the electron relaxes to valence band by emitting photons.

Since SWNTs have large unique and optical properties due to one-dimensional (1D), confinement of electronic and phonon states, called van Hove singularities in the nanotube density of state the singularities in density of state and correspondingly in the electronic joint density of state (JDOS), are related for various optical phenomena. When a van Hove singularity in the JDOS of the valence and conduct bands is matched with the energy of incident photons, resonant enhancement will occur in the corresponding photo-physical process, which is involved to the transitions to a molecular system. Therefore, resonantly enhanced Raman scattering allows this to obtain the information of vibrational properties of nanotubes.

2.1.2 Raman spectrum of SWNTs

In solid materials, the orientation related to the direction of the incident light, cannot be assumed with individual molecules. The orientation of molecule components is fixed, especially single-crystal which has an ordered arrangement of atoms. Thus, Raman spectrum will depend on atomic orientation of a single-crystal sample, and now we have the possibility to obtain information about the arrangement of the molecules in the crystal lattice [10]. This can be though in two ways; firstly when the unit cell of the structure contains more than one molecule, secondary the effective symmetry of a single component molecule and the rule of free molecules may no longer be considered. Since SWNTs are also a kind of single crystal, they are considered as a one molecule. However, in the case of crystal powder or SWNTs, the inevitable reflection of intense primary light or Raman-scattered light by the crystal powder or SWNTs, makes it more difficult to obtain high quality and intensity Raman spectrum, and also inelastic collision may also occur, which makes the photon scattered with lower frequency (low energy and intensity) as mentioned before. Therefore, excitation by laser was employed to obtain a clear and high quality spectrum. When laser excitation is used, Stokes line is emitted with a high intensity, compared to normal Raman scattering. This stimulated emission, unlike the normal Raman effect, is coherent.

Even though the laser can focus on small spots of the sample (not entire ones), resonance Raman scattering by excited laser is powerful enough to characterize the

structure of SWNTs, since different structures of SWNTs have different electronic density of state with different chiralities (*n*,*m*). This results in different energy, in singularities of SWNT and different resonance. This signal can be used to identify the (*n*,*m*) structure of SWNT. As for the resonance Raman spectrum of SWNT (Figure 2-2), there are three main important modes; tangential mode (G-band), disordered band (D-band), and radial breathing mode (RBM).

The tangential mode is the most dominant peak, which provides a signature and the nature of a carbon nanotube [11]. This peak is called the G mode from graphite. This dominant peak corresponds to a resonant excitation of in-plane optical phonons. This dominant peak appears around 1960 cm^{-1}. Since the structure of SWNTs is different that of graphite for the axial and transverse in-plane vibrational modes as shown in Figure 2-3a, the tangential G mode in SWNTs will give a multiple-peak feature, named G-band. The G-band position is slightly different in energy (different in Raman shift), indicated by the blue and red arrows. This energy difference causes energy the G-band to split into two peaks: G^+ and G^- peak, where G^+ has higher energy. The G^+ and G^- indicate atomic displacement along the tube axis and circumferential direction, respectively. The G- is caused by the curvature of the tube which has vibration in circumferential direction (Figure 2-3b).

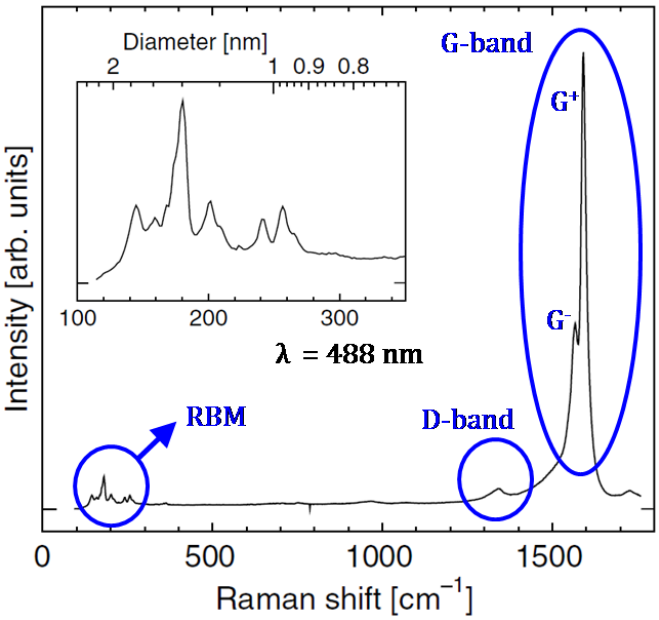

Figure 2-2 A typical resonance Raman spectrum from vertically aligned SWNTs (488 nm excitation laser). The RBM peaks are shown in the insert with dominant peak at 180 cm^{-1}, indicating vertical alignment.

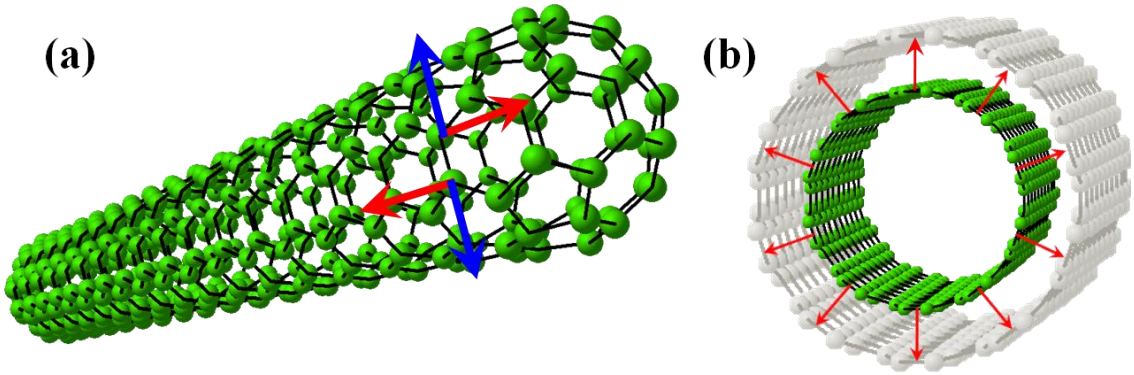

Figure 2-3 (a) the in-plane vibrational modes corresponding to the G-band Raman signal, and (b) the uniform out-of-plane vibration that gives rise to radial breathing mode (RBM) excitations.

The G^- feature can be used to identify the difference of semiconducting and metallic SWNTs. Since there is the presence of free electrons inside metallic SWNTs, the feature of the G^- is broadened, called BWF line, because of metallic character [12,13]. In the other hand, it is the Lorentzian line shape for semiconducting SWNTs.

Moreover, the excited photons can also be scattered by defects inside nanotubes, which are not crystal lattice such as, hetero-atoms, vacancies, heptagon-pentagon pairs, kinks, or even the presence of impurities (amorphous carbon), etc. Thus, the information about defects or impurities inside SWNTs can be obtained from resonance Raman spectroscopy, which is identifiable by disordered bands (D-band) around 1350 cm^{-1} as shown in Figure 2-2. As for the shape of D-band of in SWNTs, the broad feature of the peak indicates the presence of amorphous carbon, and the sharper features come from nanotubes such as, defects or non-crystalline structure. Usually, both of these features are overlapped to each other.

The last mode is radial breathing modes (RBM) (Figure 2-2). These modes usually appear in the range of 100-400 cm^{-1}, corresponding to the atomic vibration of the carbon atoms in radial direction, and can be used to confirm the presence of SWNTs in the sample. These modes are resonance out-of-plane, which vibrates perpendicular to the lattice plane and opposite to G-modes [14]. They are in resonance when the energy of the incident photons matches with the energy gap E_{ii} in the SWNT density of state. Since they resonate in the radial direction, these features can be used to characterize the diameter of SWNT (d_t) with the empirical equation,

$$\omega_{RBM} \approx \frac{A}{d_t} + B,$$

where A and B are determined from experiments. From this equation ω_{RBM} is inversely proportional to the diameter of SWNT. Thus, ω_{RBM} is higher if SWNT diameter is smaller.

Since different structures of SWNTs resonate with different excitation energies, they make RBM appear in different positions or frequencies. Therefore many different excitation energies are employed to characterize the SWNT's diameter. For vertically-aligned SWNTs (VA-SWNTs), they will have a strong RBM peak appear at 180 cm^{-1} with neighboring peaks at 160 and 203 cm^{-1}, indicating vertical alignment of morphology [15].

2.2 Optical absorption spectroscopy

The optical absorption spectroscopy, is a spectroscopic method that usually uses the wavelength of the incident light in the range of ultraviolet and visible radiation, which is the near infrared region of the electromagnetic spectrum (around 1500 - 3300 nm), called UV-vis-NIR spectral regions. The principle is based upon light propagation, transmittance or absorbance of medium or samples. From Beer-Lambert's law, the absorbance of a sample is proportional to the thickness of the sample and the concentration of the absorbing species in the sample, the intensity of absorbed incident light is found to exponentially decrease as in the equation$I(L) = I_0 e^{-\alpha Lc}$, where I_0 is the intensity of incident light, $I(L)$ is the intensity of light at optical path length L, α is the absorption coefficient and c is concentration of absorbing species in the material. The absorbance, which is related to the incident intensity, can be expressed in terms of intensity from the following equation

$$A = -\log_{10}\left(\frac{I}{I_0}\right),$$

where A is the absorbance of material at a given wavelength. Thus, we obtain the correlation of UV-vis-NIR light and absorbance for each molecule in the material, and we can use it to characterize the structure of the material. Moreover, features of absorption spectrum correspond to electronic states of materials, which can be also used to characterize electrical structures of materials, especially SWNTs with different van Hove singularities in the SWNT density of states. In the case of SWNTs, absorption probability, or absorptivity, will increase if the incident photon energy matches the energy separation with the van Hove singularities in the SWNT density of states, which are dependent upon the chirality of SWNT. Since different chiralities have different structures, size of diameter,

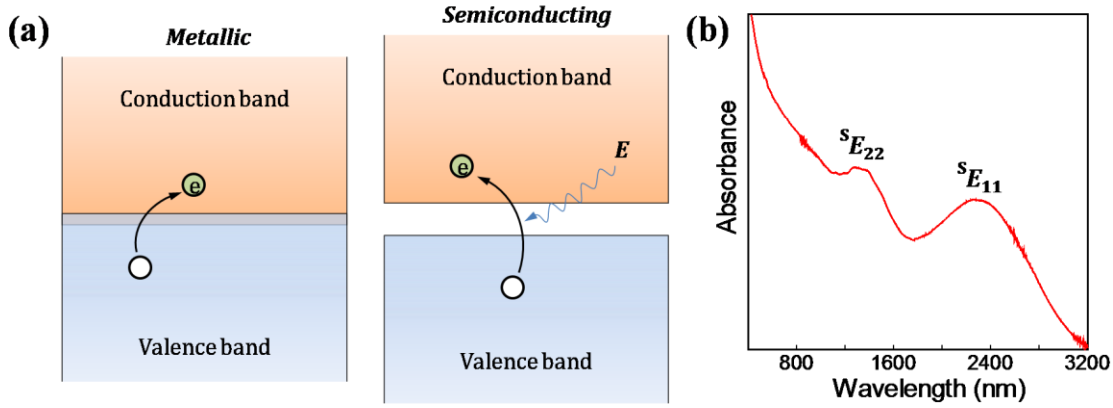

Figure 2-4 (a) Energy band gaps of metallic and semiconducting material, and (b) Optical absorption of vertically-aligned SWNTs.

semiconducting and metallic properties, energy separations are different, making absorbance are also different and all of this will show up in different absorption peaks. Thus, this measurement is one of powerful tools used for SWNT characterization.

In general, many properties of materials, especially optical properties, such as bonds or composition inside materials, have a range of optical tools that are often used to assist using the principle of optical absorption because optical properties are a direct consequence of the electronic nature of materials. In semiconducting and metallic materials (Figure 2-4a), their band structures are different because they are overlapped for metallic materials, and split out to be gaped for semiconducting ones. The electron can cross to the conduction band much easier for metallic materials, but more energy is needed to excite the electron in valence band to cross over the gap to reach the conduction band since there is small gap in between the two bands.

In the case of SWNT, 1D material, both metallic and semiconducting SWNTs also exhibit Van Hove singularities in their electronic density of state, which involve valence and conduction bands. The electrical structure is a bit different from the general materials because the transitions are restricted to symmetry considerations [16], which are depended upon the polarization of incident light to SWNT axis that results in highly anisotropic absorption. It will be strong when the polarization is parallel to the SWNT axis and weak when polarization is perpendicular to the SWNT axis. However, the transition process of the photon occurs in UV-vis-NIR range. Therefore, optical absorption spectroscopy can efficiently give information about the structure of SWNTs. One example of optical absorbance was given in Figure 2-4b.

2.3 Photoluminescence spectroscopy (PL)

2.3.1 Many forms of photoluminescence

Photoluminescence is an important technique for measuring the purity and crystalline quality of semiconductors. This spectroscopic measurement is a process in which a material absorbs photons (electromagnetic radiation) and then re-radiates photons. This can be described as an excitation to a higher energy state and then return to a lower energy state accompanied by the emission of a photon. The simplest PL processes are resonant radiations, in which photon of a particular wavelength is absorbed and an equivalent photon is immediately emitted. This process involves no significant internal energy transitions of the chemical substrate between absorption and emission. Interestingly, when the chemical substrate undergoes an internal energy transitions before re-emitting the energy from the absorption event, the fluorescence occurs. Many kinds of PL exist depending upon the aspect of fluorescence. Time-resolved photoluminescence (TRPL) is also one of the methods available. This PL is a very sensitive technique to resolve overlapping absorption signals of defects, or to distinguish emission signals by their different time decay features, where the sample is excited with a light pulse and the decay in photoluminescence with respect to time is measured. This technique is useful in measuring the minority carrier lifetime of semiconductors for elements in group of III-V.

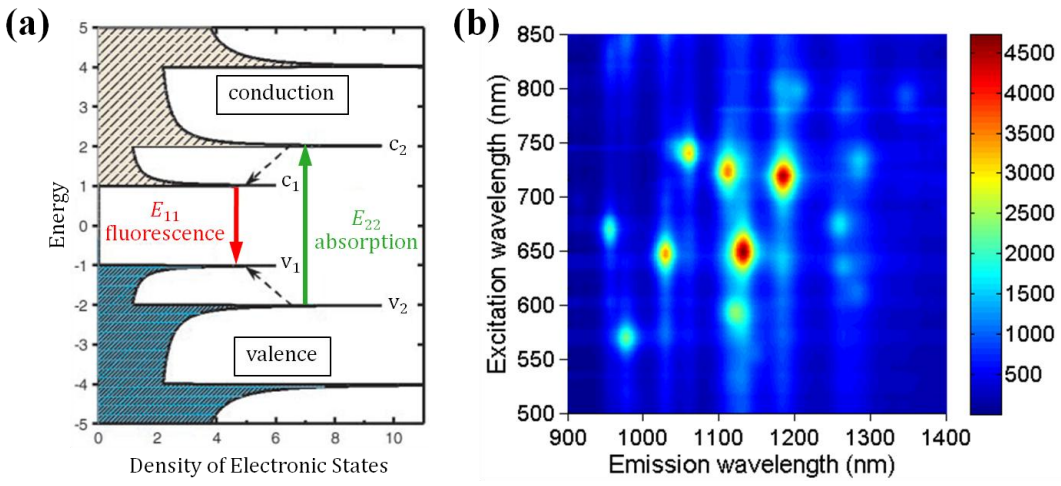

Figure 2-5 (a) Density of electronic states for a SWNT structure. Solid arrows indicate the optical excitation and emission transitions; dashed arrows denote nonradiative relaxation of the electron (in the conduction band) and hole (in the valence band) before emission. (b) The PLE map of SWNT synthesized from HiPCO process.

Furthermore, another specialized form of photoluminescence is phosphorescence, in which the energy from absorbed photons undergoes intersystem crossing into a state of higher spin multiplicity, usually a triplet state. Once the energy is trapped in the triplet state, transition back to the lower singlet energy states is quantum mechanically forbidden, meaning that it occurs much slower than other transitions. The result is a slow process of radiative transition back to the singlet state, sometimes lasting minutes or hours. This is the basis for "glow in the dark" substances. In addition, another form of PL which has a popular use is photoluminescence excitation (PLE). In the case of material as SWNTs, this PLE is used as a powerful and efficient method to characterize electrical, optical properties, specific tube structure, and chirality of SWNT, since its special 1-D structures and van Hove Singularities make them easily available.

2.3.2 Photoluminescence excitation (PLE)

As mentioned before, PL measurement has some optical limitations because it can be used to characterize semiconductors. Thus, PLE is also limited for only semiconducting SWNTs (not fluoresce with metallic SWNTs) and small-diameter SWNTs. In the Figure 2-5 [17], when the incident light is passed through the SWNT sample, light will be absorbed at photon energy E_{22} ($v_2 \rightarrow c_2$). The absorbed light is then fluorescence emitted near energy E_{11} ($v_2 \rightarrow c_2$). Meaning that PL peaks both values will vary depending upon the tube structure. Thus, in PLE map, each distinct peak corresponds to emission from the first band gap (E_{11}) of a semiconducting SWNT as shown in X-axis, which has first been excited to the second band gap (E_{22}) in Y-axis. Each peak also corresponds to specific tube of SWNT as chirality of SWNT with different peak intensity corresponding to population of SWNT in each chirality.

2.4 Electron microscopy

Electron microscopy is widely used in many fields of studies because of its necessity. This method is often used to examine morphology or thorough information of samples. There are many kinds of electron microscopy, but their principles are similar, in which wavelike nature of light is used to produce an image in a light microscope or in an electron microscope with high resolution (magnification can reach up to 100,000X depending on type of microscopes). The first simple microscopy is scanning electron microscopy (SEM) as shown in Figure 2-6a (left side), in which images are produced by scanning an electron beam over a sample in a raster pattern cross surface, and then detecting the scattered electrons (secondary electron), the emissions from the surface are then recorded. After the image is shown in 3D. However, the electron beam is not projected through the whole

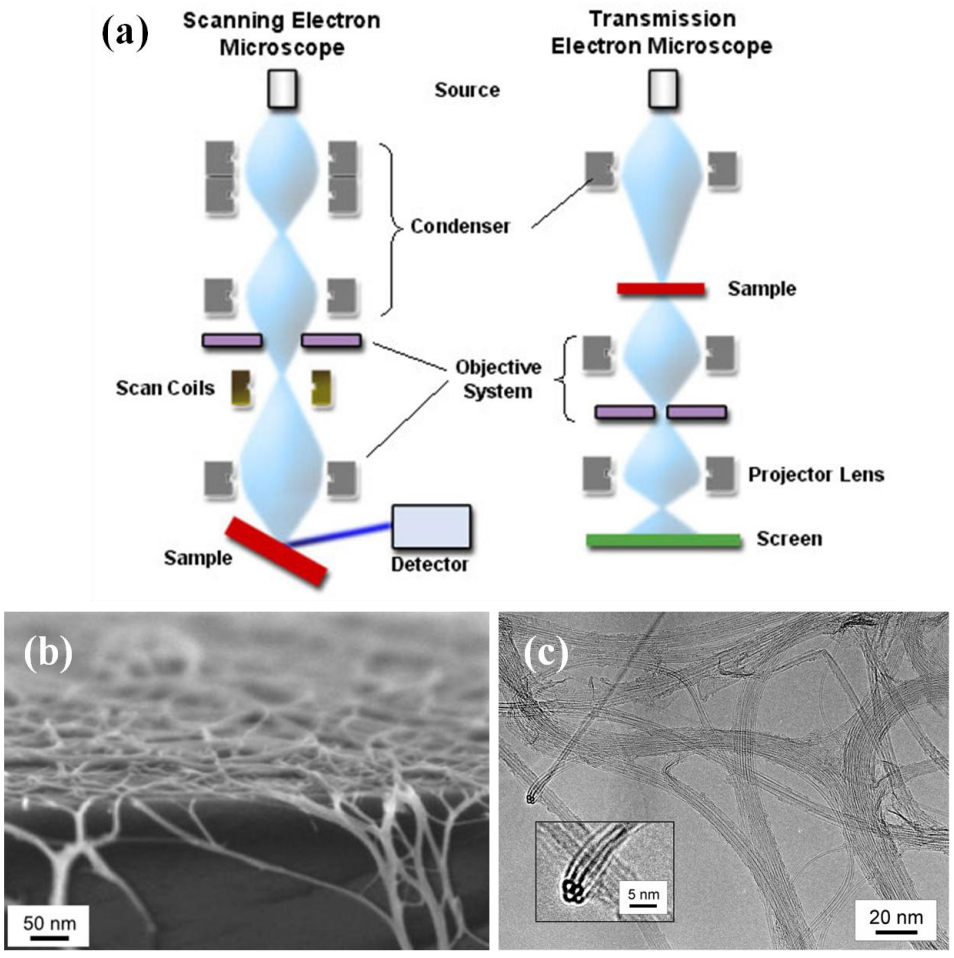

Figure 2-6 (a) The principals of scanning electron microscopy (SEM) and transmission election microscope (TEM), (b) A high-resolution FE-SEM image of SWNT bundles lying on a substrate surface, and (c) A TEM image of SWNT bundles with individual SWNTs within a bundle (in the insert).

sample area. This generates a lower-resolution image, but allows the direct mapping of surface features. Another kind of SEM, which can improve resolution, is a field emission SEM (FE-SEM) using a field emitter to obtain an intense electron beam. Figure 2-6b shows an electron micrograph of carbon nanotube bundles obtained using an FE-SEM.

Beside this one there is another kind of electron microscope (Figure 2-6a, right side) that is capable of even higher magnification (over 1,000,000X). Its principle is different from SEM. This is achieved not by detecting electrons scattered by a material, but rather by detecting electrons that have passed through the sample (transmission). This is accomplished by accelerating the electrons to high energies (typically > 100 keV) and specially preparing the sample so that it is thin enough for the incident electrons to pass through, and the resulting pattern of electron transmission and absorption is magnified onto a viewing screen. The image which is generated is a 2D map of the material's density (used to map topography in thin samples). A microscope operating on this principle is called a transmission electron microscope, or TEM. A good TEM is capable of atomic resolution, thus gives an extremely accurate picture of the crystal structure of a material. A TEM image of SWNTs produced from alcohol [21] is shown in Figure 2-6c. The single-layered tube walls can be made out in the image. A bundle of four SWNTs is shown in the inset. Since TEM can go to a very high resolution (high magnification) and can give reliable statistical information, diameter and chirality distribution of SWNT can be determined, and impurities inside sample can be also often detected.

2.5 Thermo-gravimetric analysis (TGA)

Thermo-gravimetric analysis or TGA is a simple analytical technique that measures the weight loss (or weight gain) of a material as a function of temperature. As materials are heated, they can lose weight from a simple process such as drying, or from chemical reactions, decomposition or oxidization that liberate gasses. Some materials can gain weight by reacting with the atmosphere in the testing environment. Since weight loss and gain are disruptive processes to the sample material or batch, knowledge of the magnitude and temperature range of those reactions is necessary in order to design adequate thermal ramps and hold them during those critical reaction periods. In Figure 2-7a, a sample of the test material is placed into one side of sample holders (made from platinum cup) that are supported from an analytical balance located outside the furnace chamber (fulcrum part).

The balance is zeroed, and the sample cup is heated according to a predetermined thermal cycle. The balance sends the weight signal to the computer for storage, along with the sample temperature and the elapsed time. The TGA curve plots the TGA signal, converted to percent weight change on the Y-axis against the reference material temperature on the X-axis, and also derivative of percent weight change called DTG.

Since carbon nanotubes exhibit a range of chemistries, including mixtures of different nanotube diameter, chirality, lengths together with various concentrations of metal catalysts and non-carbon nanotube impurities, TGA is employed to be utilized for bulk characterization, for determining the amount and quality of carbon nanotubes. Carbon nanotubes will be basically quantified as carbon-to-metal content, homogeneity, and detected quality (carbon-to-metal ratio, single-walled or multi-walled). TGA is one of the most straight forward methods to characterize SWNT. It can be used to directly analyze SWNTs powder to give the percentage of graphitic structured carbons (SWNT and

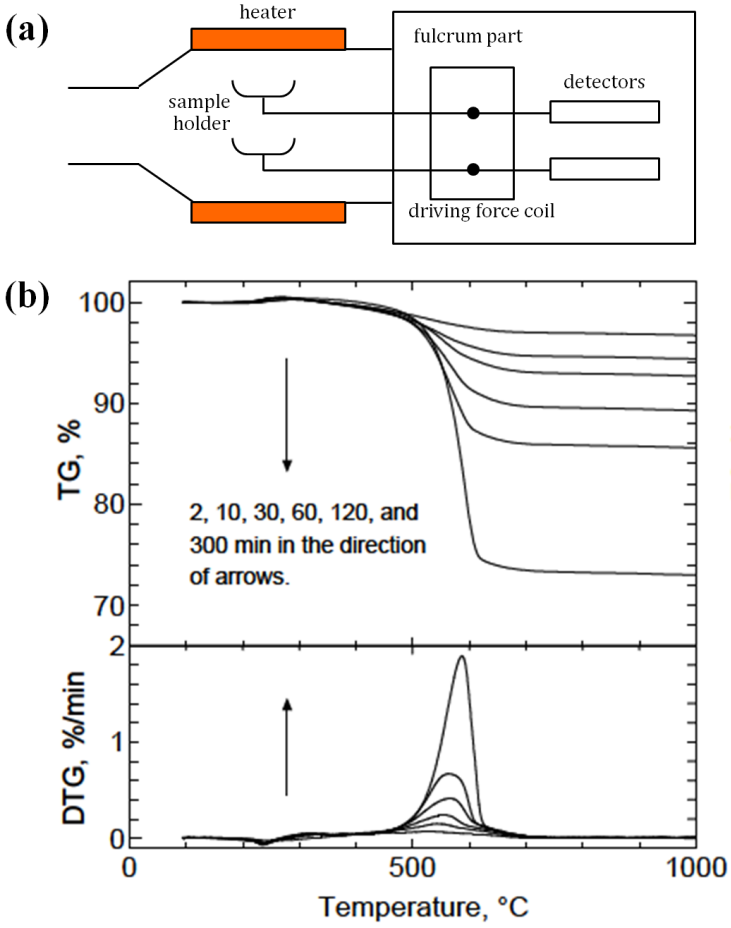

Figure 2-7 The simply operation system of thermogravimetric analysis (TGA) machine (a), and TGA and DTG curves of as-SWNT grown from zeolite particles by ACCVD.

MWNT), impurities (amorphous carbon), and catalytic metals within a bulk sample without any special requirement for preparation of sample. The percentage of catalytic metals can be quantitatively determined, while the actual percentage of different carbon forms is only semi-quantitatively determined and secondary measurement are often required to confirm TGA results. However, TGA is a destructive technique that measures mass loss as a function of temperature with carbon materials decomposing on heating.

Generally, decomposition of amorphous carbon occurs at temperature around 200 to 400˚C, which is lower than that for the decomposition of SWNTs in most of the cases, where the decomposition temperature is around 500˚C [18, 19]. After CNT samples are heated to temperatures at/or above 600°C, all carbon-containing constituents are removed, and the residual mass is comprised of catalytic metals and their oxidation products[14], MWCNTs rarely can oxidize at higher temperatures. Therefore, TGA has been used to (1) characterize as-produced SWCNT samples, (2) to track the effects of purification process [20], and (3) to monitor how changes in a manufacturing conditions affect the percentage of SWCNT within the sample. Another analysis, which is also useful for SWNT characterization, is derivative of TGA (DTG). This DTG curve can be used to determine decomposition peaks of catalytic metals, impurities and carbon nanotubes as well, as shown in Figure 2-7b.

Chapter 3

Alcohol-CVD synthesis of SWNTs

3.5 Synthesis of SWNTs

Since the SWNTs were discovered by Iijima and Ichihashi [2] in 1993, following their discovery, higher quality and with fewer defects SWNTs have been produced using improved methods, such as the arc discharge [4] and laser over methods [3]. Since for most experiments, they could not be produced in the required scale, another simple new method was developed by Hongjie Dai and his coworkers at Rick Smalley's group at Rice University. Their method consist of producing SWNTs with chemical vapor deposition (CVD) [5], in which carbon monoxide (CO) was used as a carbon source for CVD growth that reacted with the metal catalyst particles inside a heated reactor. Because it's simple and controllable, this method became the most common used for SWNT production. In the late 1990s, SWNTs were developed again by synthesis at high pressures, using CO as carbon source by Rick Smalley's group. Since this process was performed at high pressure with CO as the carbon source, it was called a high-pressure disproportional reaction of CO (HiPCO) [21]. This was the first time that gram-scale quantities of SWNTs could be synthesized with high reproducibility, and it was popular and widely used at many laboratories in the world. This process has been become important and much significant advancement has been made. Nevertheless, many challenges in nanotechnology are still out there for us to improve and investigate.

Controlling the morphology of SWNTs during synthesis is one of the critical purposes for the realization of many proposed nanotube-based applications. Beside the morphology control, the process to control the diameter of SWNT during synthesis is also another major challenge since it has been given an emphasis after many devices produced from SWNTs were developed to reach a high performance. A major advance in this area has

been made since 2003, with the synthesis of vertically-aligned SWNTs [22] using an alcohol-based CVD growth process [8]. In addition, controlling in diameter of vertical-aligned (VA-) SWNT has also been reported [23]. Not only the controls of vertical morphology structure of SWNT, but also the horizontal structure, were also realized on crystal lattice substrate [24-27].

3.6 The ACCVD method

There are many methods to achieve SWNT production, but one of common problems met is the quality or impurities of the product, which are usually amorphous carbon, multi-walled carbon nanotubes and catalyst particles that are formed during the SWNT synthesis. However, this problem was minimized when alcohol was used as the carbon feedstock gas [8], as reported in 2002. The SWNTs synthesized from alcohol, contained less impurities as shown in Figure 3-1.

Since alcohol was used as carbon source, this method was called alcohol catalytic chemical vapor deposition (ACCVD), and it has become one of the most popular methods with low-cost and high-purity of SWNTs. When alcohol is used, the reason of less-impurities is that the OH radical in alcohols reacts with carbon molecules that have dangling bonds, and result in less amorphous carbon. This OH radical also etches away carbon atoms which produce amorphous carbon [8, 19]. It is known that SWNT growth is a catalytic process, that a carbon-containing molecule reacts with a metal catalyst particle and precipitates a nanotube. The details of the growth mechanism, however, are not yet well understood. The general CVD process is still being investigated via many different methods, including molecular dynamics simulations [28].

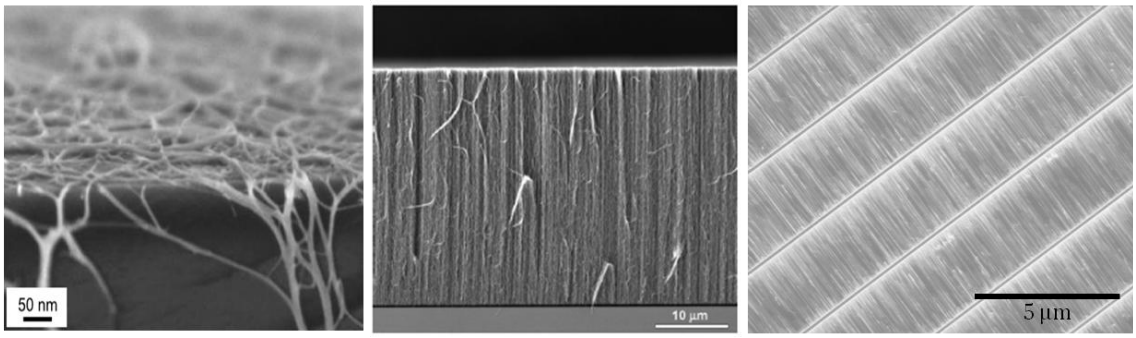

Figure 3-2 The SEM images of random, vertically-aligned and horizontal-aligned SWNT.

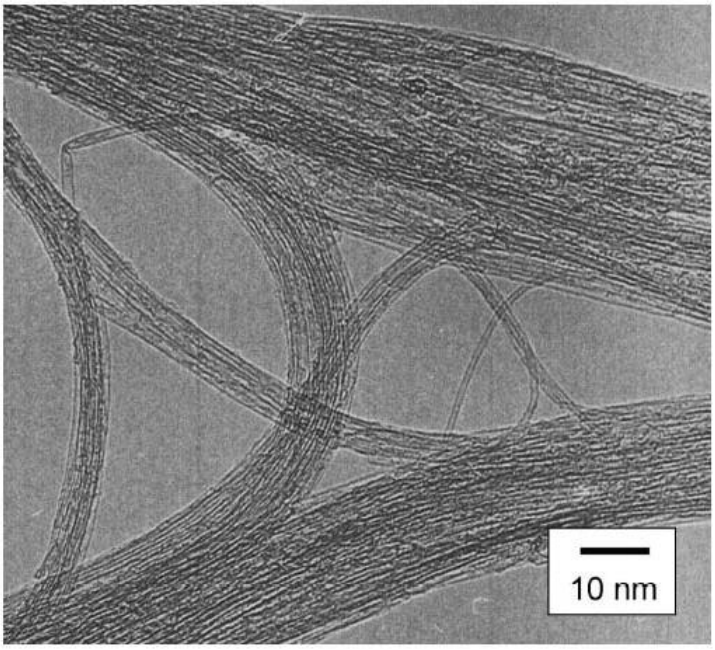

Figure 3-1 A TEM image showing bundles of high-purity SWNTs synthesized from alcohol.

3.7 Achievement of SWNTs

After the synthesis of SWNTs was achieved, via various methods, the most common methods for SWNT synthesis are found to be arc-discharge, pulse-laser vaporization, chemical vapor deposition, and high-pressure CO decomposition [29]. Due to their one-dimensionality, many properties of SWNT are anisotropic, thus control over the orientation is highly desirable for exploiting these anisotropic properties. All of these synthesis methods coupled together with advancement in SWNT research, yielded many forms of SWNT morphology that were successfully synthesized such as, random structures [29], vertical-aligned [22], and horizontal-aligned [24-27] SWNTs as shown in Figure 3-2. However, simple and low-cost methods for SWNT synthesis are in dire need, and this can be achieved by combining the ACCVD method with a liquid-based catalyst loading method [30], impregnation and evaporation method, described as follows.

3.3.1 Catalyst deposition

3.3.1.1 A liquid dip-coating

A liquid-dip coating method [30] is an easy and simple process to achieve with the result of many structures of SWNTs. The amount of catalysts deposited on the substrate surface can also be controlled by changing concentration of the catalyst. In Figure 3-3, catalyst loading was performed by submerging optically polished quartz substrate, silicon and/or crystal quartz into a separate solution containing Co acetate and Mo acetate dissolved in ethanol. The amount of each metal species in the solution was varied depending upon desired morphology of SWNTs. The substrate was immersed in the Mo solution for approximately 3 minutes, and then slowly withdrawn from the solution at 4 cm min^{-1}, followed by baking in air at 400°C for 5 min to remove the acetate and oxidize the metals. The Mo-coated substrate was then immersed again in the Co solution in which the process is the same as done with the Mo solution. The dip-coated and oxidized metal catalysts on substrate are nearly uniform with mono-dispersed catalyst particles 10^5 particles per μm^2 with diameters of approximately 1.5 nm [31]. Furthermore, formation of oxide after baking resists and prevents agglomeration of catalysts on the substrate surface at high temperature (growth temperature, e.g. 800°C).

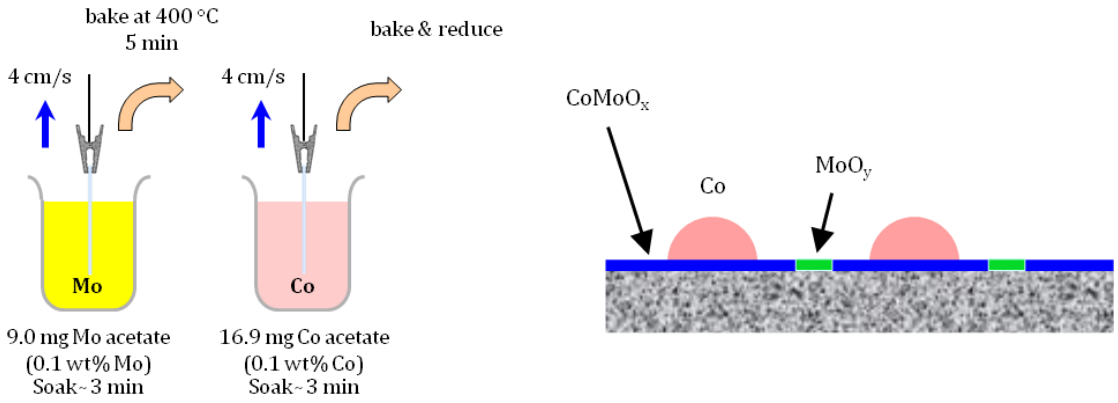

Figure 3-3 A schematic of the dip-coat catalyst loading process (left), and the chemical state of the growth surface after reduction (right).

3.3.1.2 An impregnation method

This method can be used to gain high yield of SWNTs with small diameter, but the morphology of SWNT cannot be controlled by this process. The catalyst powder can be prepared using impregnation of Co and Fe. The preparing process followed our previous report [8,19], which was developed from the procedure originally presented by Shinohara's group [32,33]. Cobalt acetate $(CH_3CO_2)_2Co\text{-}4H_2O$ (105.7 mg) and iron acetate $(CH_3CO_2)_2Fe$ (77.8 mg) were dissolved in 40 ml of ethanol along with 1 g of Y-type zeolite powder (TOSOH Corp. HSZ-390HUA, over 99% SiO_2). The percentage weight of each metal species over the total catalyst powder (i.e., zeolite + metal) is 2.5 wt%. The mixture was sonicated for 1 h in a beaker submerged in a bath-type sonicator. It was then dried in an oven at 80°C for 24 h to remove the solvent (i.e. ethanol). The resultant brown powder was ground into fine powder by a mortar and stored in oven at 80°C for future use.

3.3.1.3 Evaporation method

The uniform metal catalyst can be obtained by the evaporation of metal with slow evaporating rate under vacuum system. A substrate is fixed onto a metal plate on the upper part, and a small piece of metal wire is placed onto a tungsten boat. After this, the vacuum chamber is evacuated and set to the pressure of 2×10^{-3} Pa, then the tungsten boat is heated up through high current until it reaches the evaporating point of the metal deposited. Following that, a shutter is opened to let the metal vapor deposit on the substrate. After reaching the desired thickness, the shutter is then closed to protect the excess metal vapor. This method can be used for nanotube growth or either growth of graphene.

In the case of random and horizontally-aligned structure of SWNTs, the amount of catalyst is not necessary needed to be in high quantities to form fewer numbers of grown SWNTs. It is, on the other hand, believed that high enough catalyst density leads to SWNT growth in the vertical direction (vertical-aligned). Due to the high catalyst density, the lateral freedom of the surrounding SWNTs is limited during the growth. Thus, they are compressed to orient themselves perpendicular to the substrate and grow in an aligned aspect. As for SWNT growth by ACCVD process (Figure 3-4), the oxidized catalyst particles were reduced prior to SWNT growth by Ar containing 3% of H_2 (Ar/H_2) with a flow rate of 300 sccm and pressure of approximately 40 kPa during heating of the CVD reaction chamber. The Ar/H_2 mixture was employed to reduce the oxidized catalysts, because they are generally catalytically inactive [34]. After reaching the growth temperature, the Ar/H_2 mixture was stopped and the ethanol vapor (99.5% dehydrated ethanol) was introduced to initiate SWNT growth.

For random structures and vertically-aligned SWNTs, they can be simply synthesized by ACCVD process. After the first success of VA-SWNT synthesis, different methods have been also reported by other groups in producing this kind of forest-like structures or thick VA-SWNT, like microwave plasma CVD [35], O_2-assisted CVD [36], and etc [37,38,39,40], including water-assisted super-growth [41]. In the case of vertical growth of SWNTs, the alcohol pressures inside the growth chamber during SWNT synthesis were kept to be approximately 10 Torr (1.3 kPa) for our system, which yield an average diameter of as-grown SWNTs around 1.9-2.0 nm with several micrometers in length [42]. The critical point is how to form high density of uniformly mono-dispersed catalyst with small diameters on a substrate for achieving vertical alignment.

For the horizontal direction growth, its success has been reported by many groups by using an electric field [43-45], a fast gas flow [46, 47], and atomic steps of substrates [25, 26, 48, 49, 50, 51] with other carbon sources. Furthermore, the ACCVD method has not been used for only random or VA-SWNTs, but also for horizontally-aligned SWNTs [52]. Nevertheless, these key parameters (electric field, fast gas flow and atomic steps of substrates) are critical to align SWNTs on the substrate. When SWNTs get assembled into aligned structures, their anisotropic properties are enhanced. Therefore, such aligned structures have been used to study the fundamental properties of SWNTs; the overview will be given in a next section.

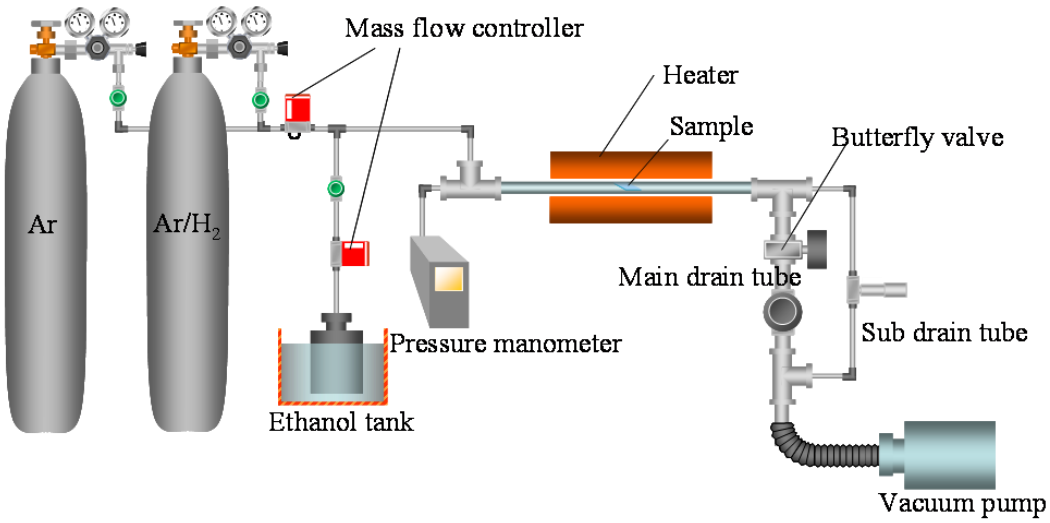

Figure 3-4 Alcohol catalytic chemical vapor deposition (ACCVD) apparatus.

3.8 Experimental procedure

The influence of various parameters, such as the ambient gas, substrate, catalyst pretreatment, catalyst recipe and the catalyst itself, was studied. SWNTs were grown on quartz and/or silicon substrates by the alcohol catalytic chemical vapor deposition (ACCVD) method [8, 53] (Figure 3-4). The influence of the synthesis parameters and their influence on the SWNT diameter were evaluated using resonance Raman spectroscopy, optical spectroscopy, scanning electron microscopy (SEM), transmission electron microscope (TEM), photoluminescence excitation spectroscopy (PLE), and thermo-gravimetric analysis (TGA). First of all, the large scale of parameters was investigated with different ambient gases. The Co-Mo binary catalysts were prepared and deposited on Si substrates by a liquid dip-coating process (Figure 3-3). The percentage of deposited Co and Mo was 0.01%wt of each. The dip-coating process was performed as shown in Figure 3-3. Substrates were dipped into Mo solution followed by baking in air at 400°C for 5 min, and repeated again with the Co solution. After the Co-Mo catalysts were annealed in air at 400°C for 5 min, dip-coated Si were placed in the ACCVD furnace, and followed by heating until 600°C under atmosphere of Ar with the pressure of 40 kPa for 15 min. Following this heating process, it was reduced by Ar/H_2 at the pressure of 60 kPa for 10 min, and heated again until 800°C under atmosphere of Ar with the same pressure of 40 kPa for 10 min. After the temperature reached 800°C, the ethanol was introduced to the

ACCVD chamber with the pressure of 1.2 kPa for 5 min, followed by cooling with Ar gas. The same experiments were also performed with the same procedures by replacing the Ar during the heating process with two different ambient gases (He and N_2, respectively). To obtain the optical spectra and PLE spectra, as-grown SWNTs were dispersed in 2 ml of D_2O with 0.1 g of sodium deoxycholate (DOC) with bath sonication for 1 h, and an additional 20 min of ultra-sonication. This suspension was then centrifuged for 30 min at 8500 rpm, 6623g and the supernatant was extracted for measurement.

Furthermore, aluminum (Al) was deposited on the quartz substrate by the evaporation method with 10 nm of thickness, followed by annealing in air at 400˚C for 5 min to form metal oxide layer of aluminum (Al_2O_3). The Al_2O_3-coated substrate was then deposited with 1 nm of Co and Al (2 nm), respectively. It was annealed again at the same temperature for 5 min. Following this catalyst deposition, the catalysts-coated substrate was reduced at 600˚C for 15 min by Ar/H_2 under pressure of 60 kPa. The thick SWNT arrays were synthesized at 800˚C for 10 and 120 sec. The Al_2O_3-coated substrates were also reduced at different temperatures (400-600˚C) to investigate the influence of reduction.

In addition the influence of the ambient gas and supporting materials, the pre-treatment of catalysts, was also carried out to deliver smaller scales of parameters. As for the catalysts pre-treatment, the Co-Mo binary catalysts containing 0.01%wt of each

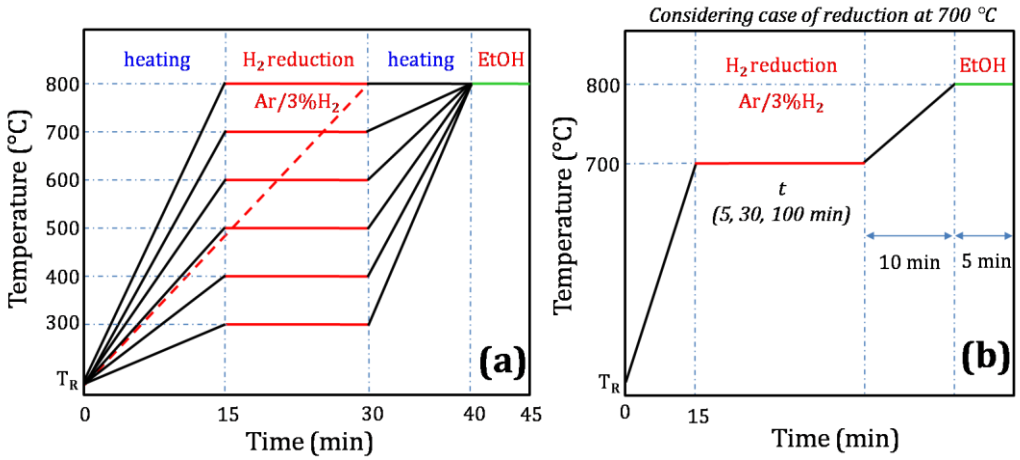

Figure 3-5 a) Temperature profiles of different catalyst reduction processes (dash, dark and dot line represent heating, H_2 reduction at certain temperature and continuous H_2 reduction process, respectively), b)

metal species were deposited onto the substrates by the same method as the previous experiment (Figure 3-3). The reduction process was modified to reduce the Co-Mo binary system at different temperatures—ranging from 300 to 800°C—by Ar containing 3% H_2 (Ar/H_2) under the pressure of 60 kPa. The different heating and reduction stages are shown in Figure 3-5a. Following this reduction, SWNTs were synthesized at 800°C for 5 min. The results from this reduction process were compared to the case of continuous H_2 reduction, in which Ar/H_2 was present throughout the heating process at a pressure of 40 kPa and a flow rate of 350 sccm (typical CVD). Furthermore, time-dependence of H_2 reduction was also investigated by extending the reduction time with a fixed temperature. SWNTs were then synthesized with temperature-programmed reduction at 700°C. The Co-Mo binary catalysts were reduced for 5, 30 and 100 min. Based on typical CVD, instead of using only Ar/H_2 as a reducing gas, small amount of distilled water (100 µL of H_2O) were introduced into the CVD system to investigate the influence of water on the diameter of SWNTs. Firstly CVD chamber was closed after evacuating any gas species inside the system. This small amount of water was introduced into the CVD chamber at a temperature of about 100 °C (with approximately 2.5 kPa) while the CVD chamber was heated to 800°C. Following this process, Ar/H_2 was also introduced into the chamber with pressures of approximately 40 kPa. At CVD growth temperature (i.e. 800°C), water and Ar/H_2 were removed from CVD chamber before introducing the ethanol with pressures of approximately 1.2 kPa for 5 min.

Apart from this, the transformation of the catalyst was also investigated by changing the catalyst recipe. This can be performed by varying the catalysts concentration, substrates were prepared by a liquid dip-coating method using cobalt (Co) concentration varied from 1 to 1/128 times of 0.01%wt Co metal with fixed percentage of Mo metal (0.01%wt), and different molybdenum (Mo) concentrations (1/2 – 5 times of 0.01%wt Mo) with fixed amount of Co metal (0.01%wt). Followed by continuous reduction (typical ACCVD), they were annealed under Ar containing 3% of H_2 (Ar/H_2) with a flow rate 300 sccm, so that the pressure inside was maintained at 40 kPa. After the temperature reached 800°C in 30 min, it was then stabilized in another 10 min, and Ar/H_2 was then stopped. Finally, the ethanol was introduced for 5 min at pressure of 1.2 kPa, followed by cooling with Ar/H_2. The effect of the different binary catalysts ratios on the diameter of SWNTs was evaluated mainly by optical absorbance and resonance Raman spectroscopy.

To investigate the influence of the catalyst on the diameter of SWNT, a new noble transition metal was used in the bimetallic catalyst. Rh (0.01%wt) was used instead of Mo in the dip-coating process. The catalyst was then reduced under continuous H_2 supply, followed by synthesis from ethanol at 800°C for 10 min. Resonance Raman spectra and SEM micrographs of the resulting SWNTs were compared with those from SWNTs synthesized using the standard Co-Mo system. The USY-zeolite powder was also employed to support Co-Rh binary catalysts. The catalytic powders was prepared according to reported procedure [8,19] using the impregnation method, and the concentrations of each metal were 2.5 %wt. SWNTs grown from this catalytic powder at 800˚C were compared with that grown from Co-Mo and Co-Fe supported by zeolite and also HiPCO SWNTs [21]. As-grown SWNT powder was additionally characterized by thermo-gravimetric analysis (TGA), as well as, photoluminescence excitation (PLE) spectroscopy. TGA was performed with a heating rate of 1˚C/min under a 100 sccm flow of N_2. To obtain PLE spectra, dispersed SWNTs were prepared with the same method as mentioned before.

Chapter 4

Synthesis and diameter control of SWNTs

Since SWNTs are one of the most versatile nanomaterials in the world with many good properties [54], with uses ranging from their bulk use for strengthening composites to use of individual nanotubes for biomedical and electrical applications, the properties and structure of SWNTs have been widely studied. It has been well recognized that the properties and structure of SWNTs are strongly dependent on the chirality. To achieve chirality control of SWNTs we need to closely carry out the control of the diameter of SWNTs, since a number of chirality of SWNTs is lower with narrow diameter distribution or smaller in diameter of SWNT. The diameter control of SWNT with controlled structures has been studied by many researchers [3-5, 7, 22, and 47]. Among these methods, chemical vapor deposition (CVD) process is the dominate method for SWNT synthesis, which has a great potential in term of quantity and good control over the product [5]. Furthermore, SWNTs with small diameter (approximately 1 nm) have a larger band gap, and also are more mechanically stable than larger diameter SWNTs. This make smaller diameter SWNTs important for many kinds of devices. In this work, I investigated many methods to achieve diameter control of SWNT from a macroscopic viewpoint (i.e. environment gases, substrate) to a smaller scale (i.e. catalysts).

4.6 Ambient gas effect

Since the gas environment during SWNTs growth can affect the catalyst structure and/or properties [55], used to synthesize SWNTs, the ambient gas is one of key parameters to achieve structure control of SWNTs. Moreover, in order to avoid the direct

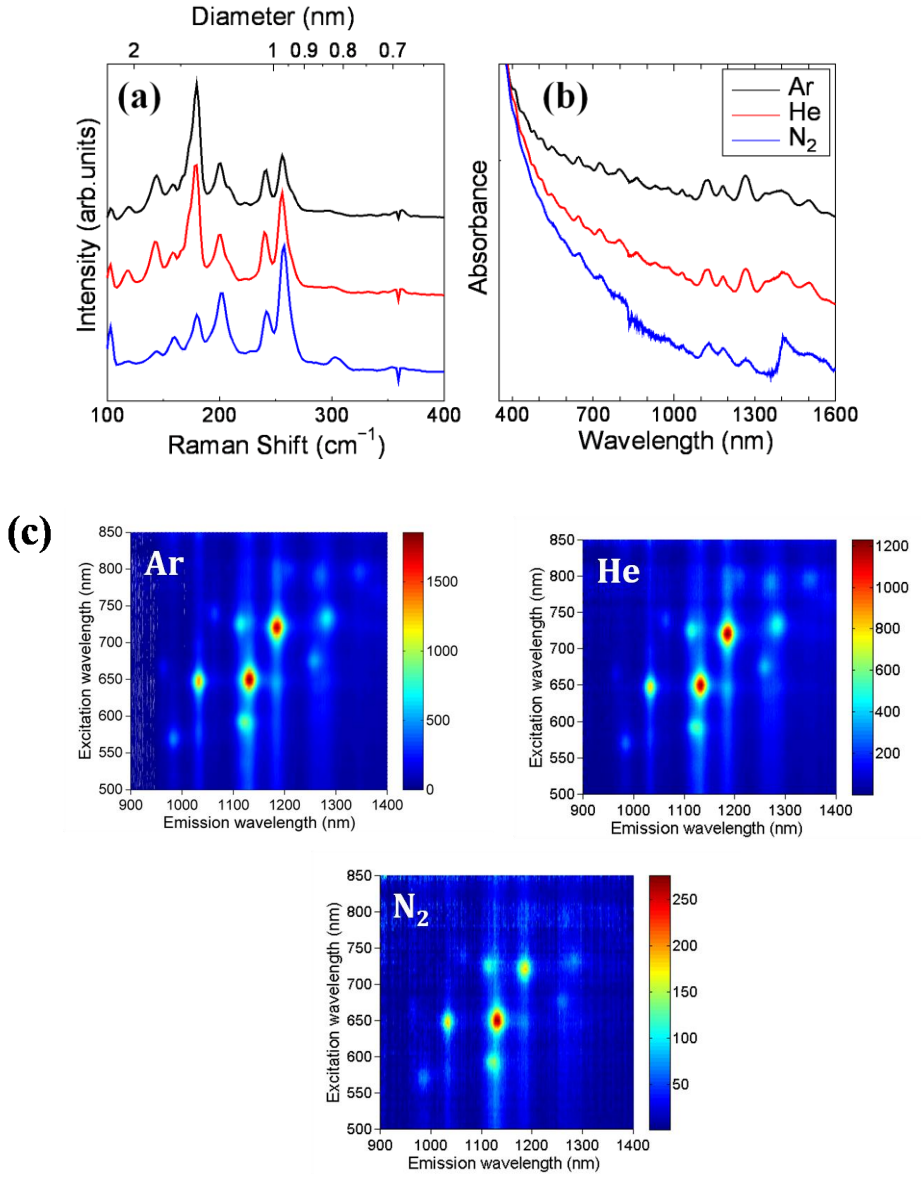

Figure 4-1 (a) The RBM region of resonance Raman spectra, (b) the optical absorbance spectra, and (c) photoluminescence excitation (PLE) maps of SWNT grown from catalysts annealed with different ambient gases.

reaction with the catalyst during the nanotube growth, the carrier gas often used is Ar and He.

In this section, the influence of ambient gases (Ar, He and N_2) on the diameter of SWNT was investigated through ACCVD process. Figure 4-1a compares RBM peaks from resonance Raman spectroscopy (100-400 cm^{-1}) of SWNTs grown from catalysts annealed with different ambient gas (Ar, He and N_2). The sharp peaks indicate the presence of SWNTs, with two strong peaks at 145 and 180 cm^{-1} existing in all cases, indicating vertical-aligned morphology. The trend of smaller diameter is clearly seen in the RBM

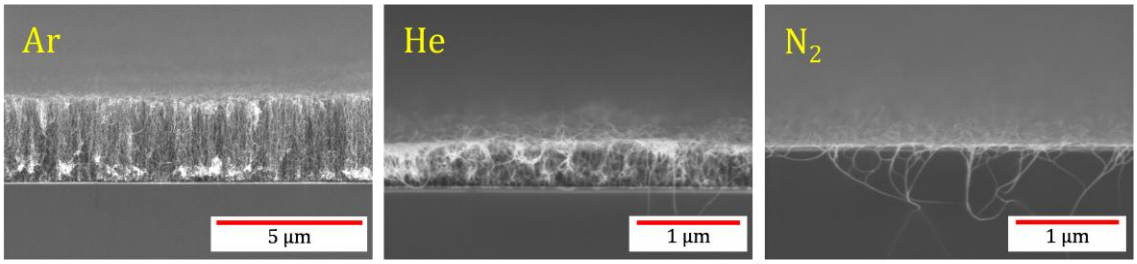

Figure 4-2 The SEM images of SWNTs grown catalysts annealed with different ambient gases.

region, indicating that the diameter of SWNTs grown with N_2 can be reduced to smaller values than with He and Ar, respectively. However, the results from optical absorbance (Figure 4-1b) remain unchanged which is indicated by the position of E_{11} and E_{22} peaks. This indicates that although more small-diameter SWNTs may have been synthesized with N_2, the percentage of these nanotubes in the entire sample is still small. It should be also noted that mean diameter and diameter distribution of SWNTs in the entire sample should be obviously presented by optical absorption. This result was confirmed by photoluminescence excitation (PLE) map as shown in Figure 4-1c, measured from suspended SWNTs. The fluorescence emission wavelength range was recorded from 900 to 1400 nm, while the excitation wavelength was scanned from 500 to 850 nm in 5 nm steps. Each peak in the PLE map corresponds to emissions of the first electrical band gap (E_{11}) of semiconducting SWNT, first excited to second electrical band gap (E_{22}). The PLE map indicates the chirality distribution is similar for Ar, He and N_2. This might be possible that catalysts were not reacted or there were no change in agglomeration of catalyst under different ambient gases during heating, since no presence of H_2 reduction during heating up, where ambient gas are different.

The result from Harutyunyan's group [56], they claim that only metallic SWNTs can be obtained by using He as the noble ambient gas during thermal annealing of the catalyst, in which catalyst shapes are changed to facet shape, and it is critical to produce more metallic SWNTs (maximum of 91%). However, H_2 and H_2O were still involved during annealing, which might also influence the catalyst properties not only He itself. From my results, the influence of ambient gas does not have any affect neither on reducing SWNT diameter nor producing more metallic SWNTs. Nevertheless, the yield of SWNTs (presented by the SWNT's film thickness as shown in Figure 4-2) was changed after ACCVD process through different ambient gases during thermal annealing. The SWNT yield grown from catalysts annealed with Ar, can produce thicker nanotube films than that with He and N_2, respectively. The thinnest nanotube film can be observed by introducing

N_2 during thermal annealing. This might be because in the presence of N_2, atomic nitrogen N derived from N_2 might be a poison to the catalyst activity, catalyst structure, or the cracking of the catalyst [57]. Ar and He are, however, inert gases, which have no influences on catalyst activity. Another possible reason of thicker films in the case of Ar and He might be from different thermal conductivities. Since He has much higher thermal conductivity than Ar, He can bring out more heat during thermal annealing than Ar, and temperature of catalysts can be lower before ACCVD growth at 800˚C. This will induce different growth temperatures, resulting in different yield of SWNTs.

4.7 Influence of the supporting substrate

Although the VA-SWNT arrays can be achieved on a flat substrate [58] (i.e. quartz and Si), the diameter of as-grown SWNTs are still difficult to control since catalysts can easily move around and aggregate on flat surfaces. Thus, supporting materials have been employed to control the SWNT diameter such as using zeolite particle [8, 19], MgO [59, 60], SiO_2 [61], etc. Furthermore, another supporting material, which has been often used, is aluminum oxide (Al_2O_3). It has been used to gain the yield of VA-SWNTs [41] and also to reduce the SWNT diameter [37]. Therefore, the effect of Al_2O_3 supported on flat quartz substrates on SWNT diameter was carried out.

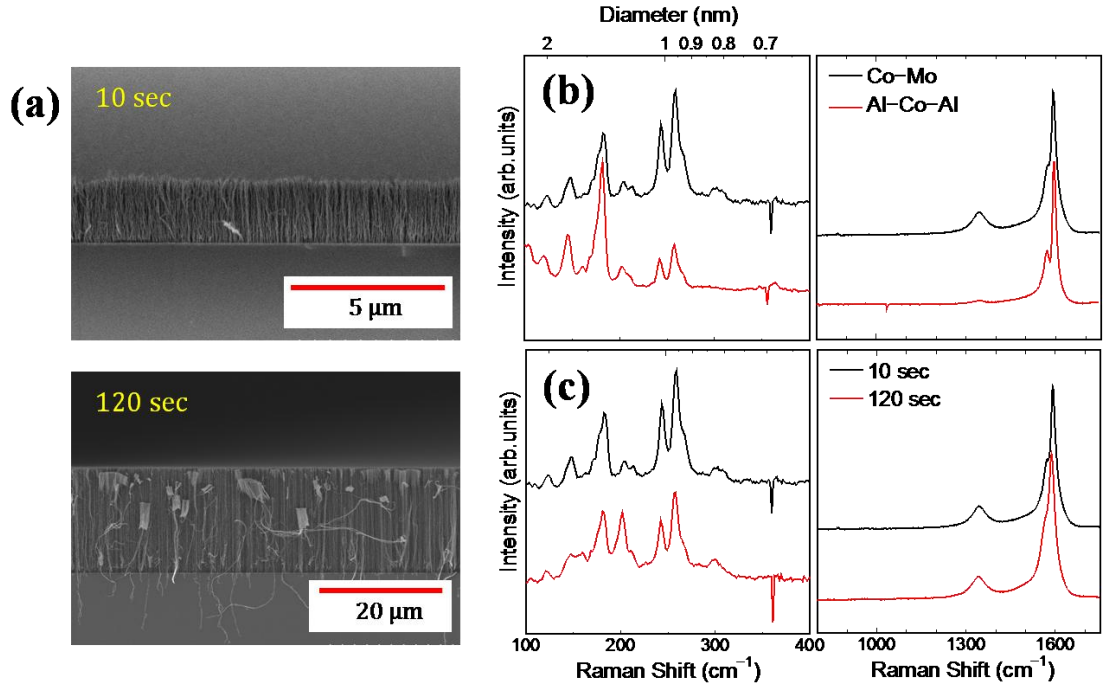

Figure 4-3 The SEM images (a), and Raman spectra of VA-SWNTs grown for 10 (b) and 120 sec (c).

From SEM images as shown in Figure 4-3a, the aluminum oxide support can gain the yield of VA-SWNTs (presented as the film thickness) from our condition. The thickness of as-grown VA-SWNTs array was extremely increased and more than 20 μm can be obtained in 2 min, in which the growth rate was 10 μm/min. The yield of SWNT is much higher compared to our previous reports [62]. From the RBM regions (100-400 cm^{-1}) in Figure 4-3b, the RBM peaks around 180 and 200 cm^{-1} indicate the presence of VA-SWNTs array. The diameter of SWNTs seems to be clearly smaller than SWNTs grown from Co-Mo catalysts, indicated from the higher intensity of the smaller-diameter peaks around 250 cm^{-1}. Nevertheless, VA-SWNTs still lack perfect crystalline look, indentified by strong and high intensity of the D-band (Figure 4-3b). In addition, the splitting out of the G^- peak from the G^+ cannot be observed. This might indicate the existence of high population larger diameter SWNTs in the sample, which is not resonating in the RBM region, even though the smaller diameter peaks can be clearly seen in the RBM region.

As for the mechanism of VA-SWNT growth, the diameter of SWNT from the top could be smaller than the one at the root. The nanotubes in the top part were investigated by reducing growth time from 2 min to 10 sec with the same ACCVD procedure, where the early growth stage is thought to be. From resonance Raman spectroscopy of early stage growth of SWNT (Figure 4-3c), we can see SWNTs were still grown in the vertical fashion as seen from the peak at 180 cm^{-1}, and the clear difference can be seen at the peak around 200 cm^{-1}. Additionally, the intensity of the smaller-diameter peak around 250 cm^{-1} is also higher than that of 2 min growth, showing the presence of smaller diameters for the growth at early stage.

In addition to the reduction process of SWNTs grown from dip-coated Co-Mo, the reduction of Co supported on alumina was also investigated. The thickness of VA-SWNT

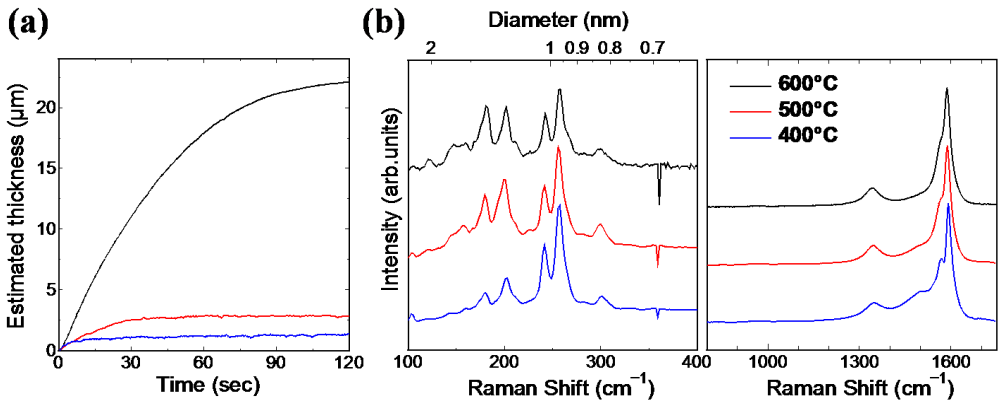

Figure 4-4 (a) Growth curve, and (b) resonance Raman spectra of SWNT grown from Co catalysts supported on Al_2O_3 and reduce at different certain temperature.

array was decreased by decreasing the reduction temperature as in the previous result. Figure 4-4a shows *in-situ* measurement of VA-SWNT array thickness with different reduction temperature ranging from 400-500°C. It is obvious that reduction at 600°C can produce thicker nanotube films. With a higher reduction, however, it is clearly seen that SWNT diameter is larger than lower reduction temperature as shown in Figure 4-4b. The RBM peak around 250 cm^{-1} indicates smaller diameter of SWNT that become dominant with lower reduction temperature. Furthermore, the G^+ and G^- peaks are obviously split out when using 400°C reduction, confirming the presence of smaller SWNT diameter. Nevertheless, it should be noted that modifying the reduction condition does not improve the crystallinity of SWNTs, as seen from the unchanged in intensity of the D band.

4.8 Influence of catalysts pre-treatment

4.3.1 Catalyst reduction

The continuous H_2 reduction during heating until the growth temperature is reached has been the standard for the synthesis of vertically aligned SWNTs (VA-SWNTs). However, we expect the reduction can be better controlled if it is performed at a fixed temperature, thus eliminating the dependence of temperature profile during reduction. Figure 4-5 compares resonance Raman spectra of SWNTs synthesized after reduction by H_2 at a constant heating rate and from reduction at different fixed temperatures. Sharp peaks appearing in the radial breathing (RBM) region (100-400 cm^{-1}) indicate the existence of SWNTs. Two strong peaks at 145 and 180 cm^{-1} appear when nanotubes grow in the direction normal to the substrate, and represent the case of continuous H_2 reduction [15]. This can be interpreted as the morphology of SWNTs is still vertically aligned when H_2 is introduced during the entire heating time, and for fixed reduction temperature intervals between 500 and 800°C. The latter is because the reduction becomes more aggressive at higher temperatures and reduces enough of the catalyst particles to reach the areal density necessary to achieve vertical alignment. Randomly oriented SWNTs were obtained for reduction temperatures lower than 500°C, as shown in Figure 4-6. Interestingly, the RBM region also shows that the diameter of SWNTs tends to decrease for lower reduction temperatures. This might be because of the reduced diffusion and agglomeration of catalysts particles at lower reduction temperatures. This trend was also observed in UV-Vis-NIR absorbance spectra (Fig. 4-7a). Figure 4-7a shows the first optical band gap (E_{11}),

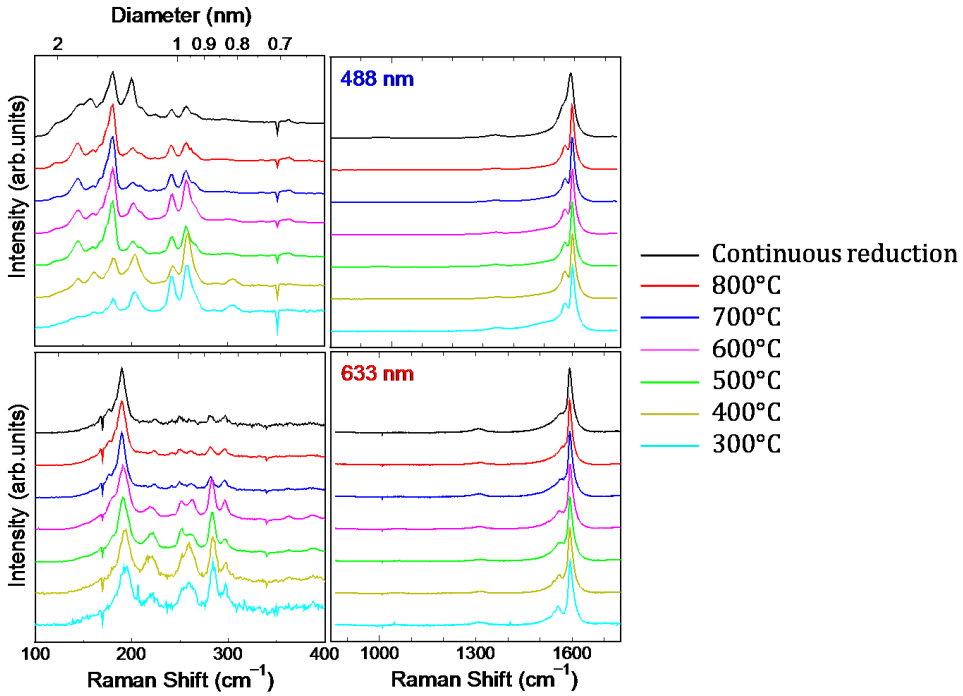

Figure 4-5 Resonance Raman spectroscopy of as-grown SWNTs for each reduction condition compared with the case of continuous reduction.

which can be used to indicate a mean diameter of SWNTs, that was slightly blue-shifted for a reduction at lower temperatures. Figure 4-7b shows the relation between the mean SWNT diameter, which was determined by optical absorbance [63], and different reduction temperatures. We find a slight decrease in SWNT diameter for lower reduction temperatures. In addition, the change in reduction time was carried out to investigate its influence on diameter and morphology of SWNTs. Since the difference in diameter of SWNT is not always obvious from resonance Raman spectra because it may not be representative of the entire sample, resonance Raman spectra of SWNTs grown from different extended reduction are not different. However, UV-vis-NIR spectra indicate the

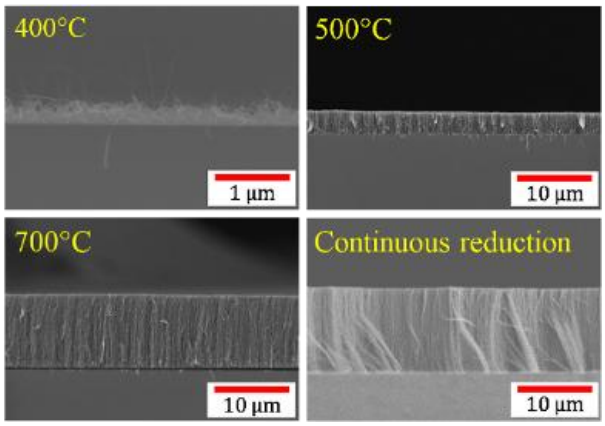

Figure 4-6 The SEM images of SWNTs grown at different fixed reduction temperature.

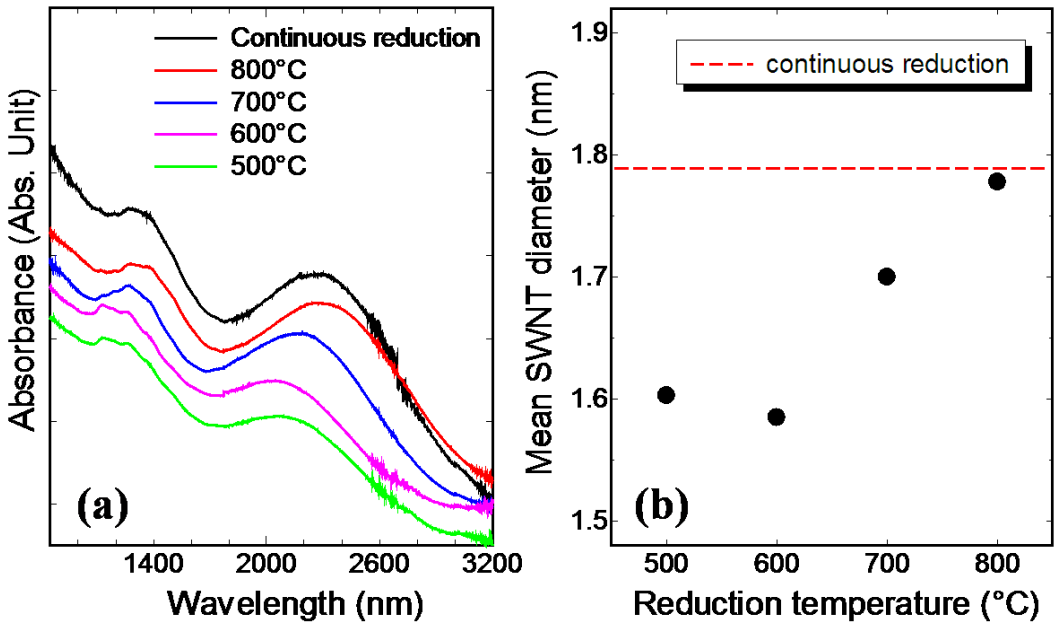

Figure 4-7 (a) The optical absorbance of as-grown SWNTs synthesized from different reduction temperature, (b) Influence of reduction temperature on mean diameter of SWNTs synthesized by ACCVD.

diameter of the SWNTs increase after extended reduction at a given temperature (not shown). Furthermore, the SWNT film thickness was reduced by extended reduction time (not shown).

4.3.2 Water-assisted catalysts annealing

Chemical vapor deposition (CVD) has been become the standard and well known method for SWNT synthesis. Adding a small amount of water in this process during the nanotube growth has been well known as the super growth method [41]. The small amount of water was sometimes introduced during CVD growth together with the carbon source to narrow the SWNT diameter distribution, extend catalyst-life time and/or gain higher nanotube yield [41, 64, and 65]. By employing ethanol as a carbon source, water is, produced from the ethanol during the CVD growth at high temperatures. Thus, water might be produced in larger volumes during the growth process when water is put into a chamber together with the ethanol. As for the results in the previous section, the catalyst pre-treatment before CVD reaction was presented. In addition, Dugulan's group [66] reported that the size and diameter distribution of Co catalyst can be reduced by exposing H_2O, H_2 and Ar together. Thus, water-involved pre-treatment was gained to achieve the diameter control of SWNT.

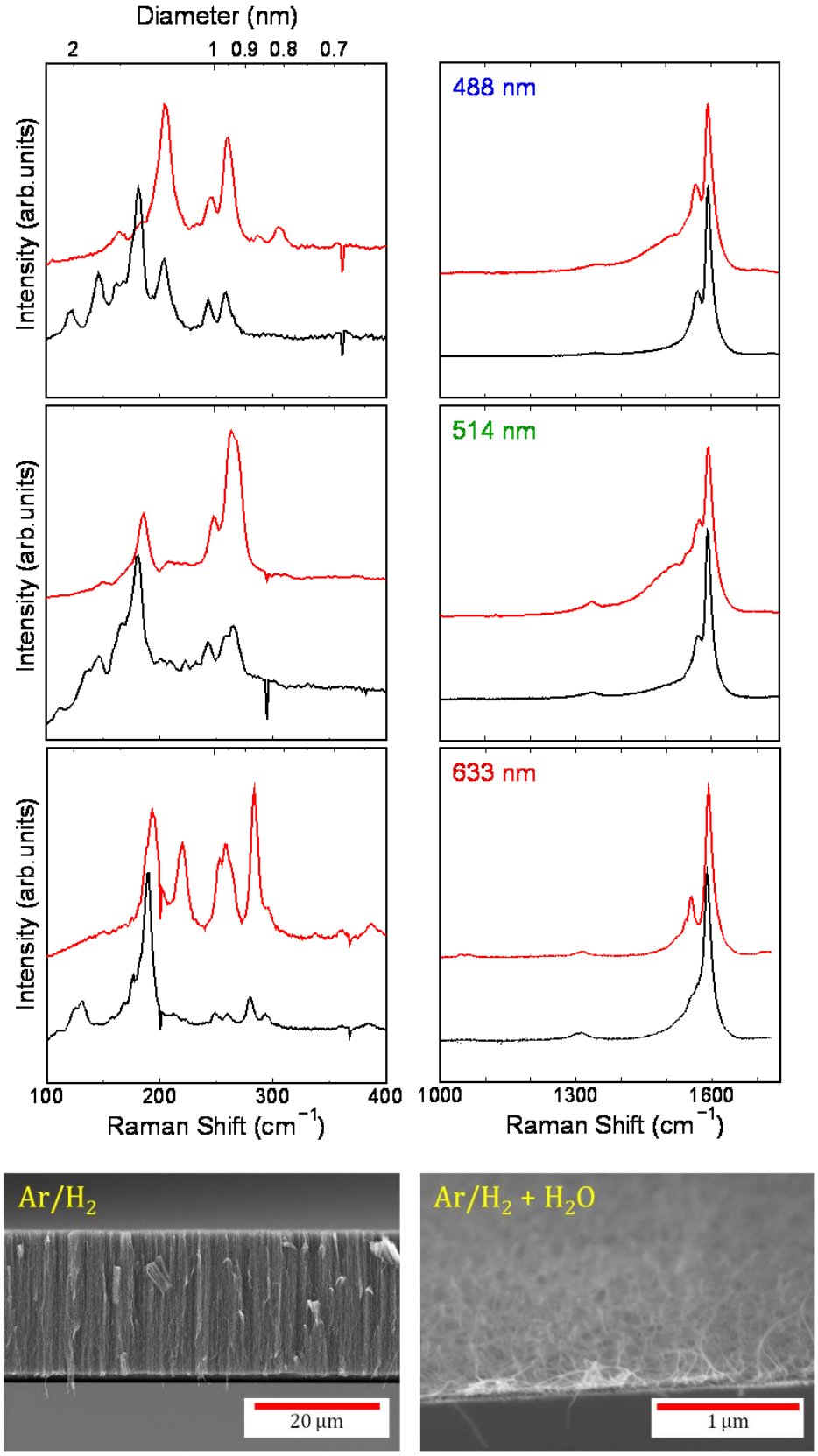

Figure 4-8 (a) Resonance Raman spectra (red and black solid line represent treatment with and without H_2O during annealing), and (b) the SEM images of SWNTs grown from Co-Mo catalysts treated with and without additional H_2O, indicating the change in diameter and morphology.

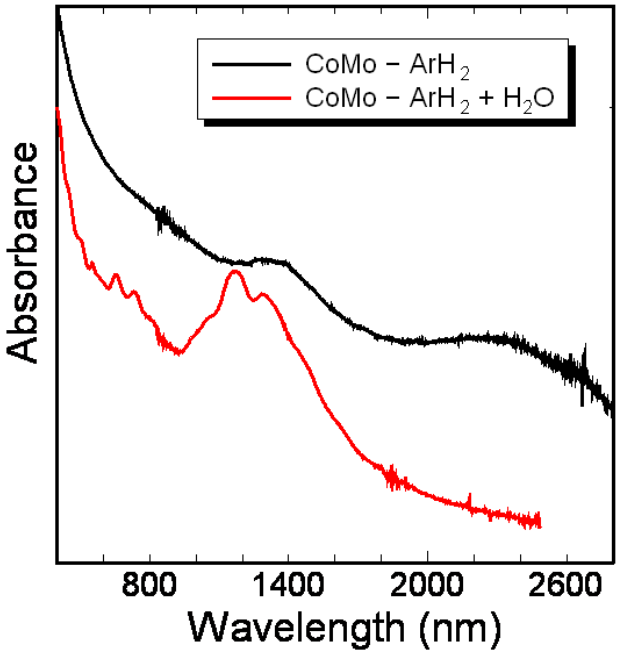

Figure 4-9 The optical absorption spectra of as-grown SWNTs grown from Co-Mo catalysts treated with and without additional H_2O, shows clear different in diameter.

Figure 4-8a shows resonance Raman spectrum of SWNTs grown from water-assisted pre-treated catalyst, compared to that without water assist (hereafter called normal condition), which was characterized with three different excitation energies. The RBM region (100-400 cm^{-1}) indicates the presence of SWNTs. From a 488 nm excitation wavelength, the intensity of the small-diameter peak around 200 and 250 cm^{-1} is higher than SWNTs grown in normal conditions. The Breit-Wigner-Fano (BWF) features in the G-band region in the water-assisted case, indicating an increase in the population of small-diameter metallic SWNTs, which is consistent with the high intensity of RBM peak around 250 cm^{-1}. Moreover, this can also be clearly seen from the Raman spectra with other excitation wavelengths (514 and 633 nm). The smaller-diameter peaks (i.e. 250 - 400 cm^{-1}) are prominent. Additionally, the G^- feature is obviously split out from the G^+ feature.

Figure 4-8b shows SEM images of SWNTs grown from both cases on quartz substrate, indicating the morphology change from a vertical fashion to a random orientation. Since the morphologies of SWNTs in both cases are totally different and this difference will cause differences in the intensity of Raman peaks, optical absorption measurement (Figure 4-9) was employed to characterize the mean diameter of SWNT over the entire sample. The shift in diameter of SWNT can be clearly seen from the optical absorption spectrum. The position of E_{11} peak was extremely shifted from 2400 nm to higher energy (lower

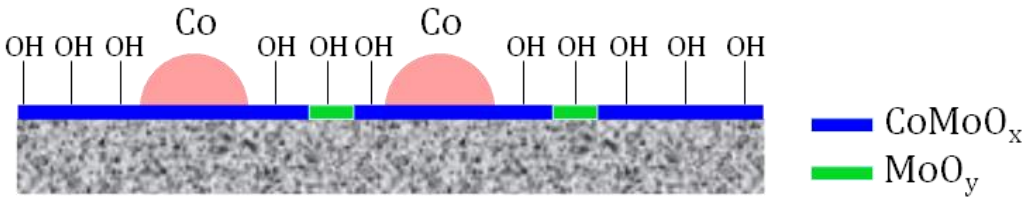

Figure 4-10 The model of the OH radical bonding formed on the metal oxides layer.

wavelength) around 1200 nm, which corresponds to the E_{22} position around 750 nm, compared to normal conditions.

These results agree with Dugulan's group [66] in term of SWNT diameter change that is depended on the size of the catalyst. This can be explained by the role of water during the annealing (pre-treatment) which is to keep the size of Co particle during sintering. It might be because of OH radicals produced during the heating process [67], in which surface hydroxyl (hydrogen on the metal oxide) is produced from the reaction between water (H_2O) and metal oxide (*O*), H_2O + *O* ↔ 2OH*, that reduces the catalysts aggregation. Based on the chemical state of Co-Mo catalyst as shown in Figure 4-10, surface hydroxyl is formed onto the area of metal oxide (i.e. $CoMoO_x$ and/or MoO_y). In the other hand, in the case of using normal conditions, there are no sources to produce OH radicals during the heating process. Thus, agglomeration of catalyst cannot be reduced to result in small diameter of SWNTs.

4.9 Effect of catalyst recipe

Since the diameter control of SWNT has been given an emphasis for the achievement of controllable SWNT structures, there are many groups of variables that have controlled the SWNT diameter, including the environment effect such as, ambient gas temperature, pressure, flow rate of carbon source, *etc.* Since they still have some limitations when it comes to controllable SWNT diameters, they are strongly depended upon the size of the catalyst [68]; directly controlling the catalyst size is the most straightforward approach for diameter control of SWNT. There are many methods to achieve this purpose by adjusting not only the supporting substrate, but also the catalyst preparation. By using supporting substrate such as zeolite, the size of the catalyst particle is restricted on substrate; on the other hand, the nanoparticles can easily move around, migrate and aggregate at high

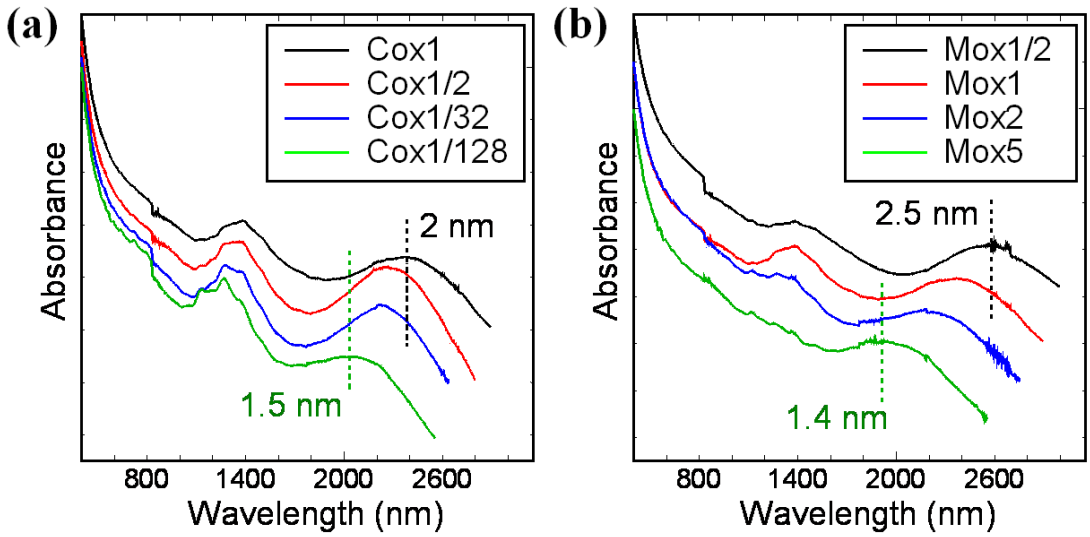

Figure 4-11 The optical absorption spectra of aligned SWNTs grown from different catalyst recipe with Co and Mo concentration dependence.

temperature during the CVD process. Therefore, controlling the diameter of SWNTs on a flat substrate is one of the most challenging works. Moreover, molybdenum [31] (Mo) or alumina [41] (Al) are also one of the other supporting species, which have been often used and deposited on the surface of substrates as intermediating layers to suppress migration of the metal catalyst nanoparticles.

Based on our previous work [31], in Co-Mo binary catalysts system Mo acts as a supporting material and stabilizes Co nanoparticles on flat substrate. Although Co is the

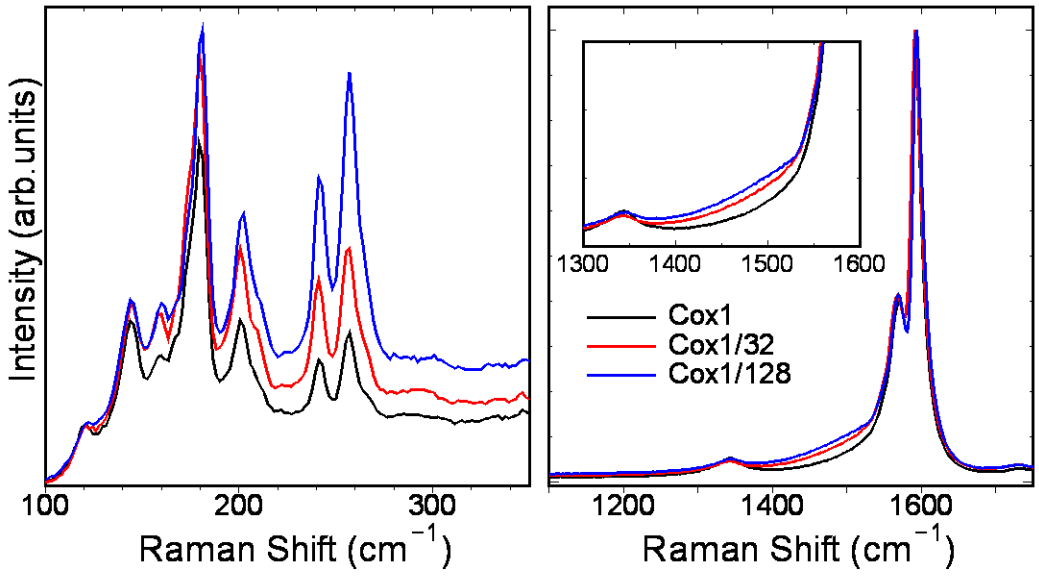

Figure 4-12 Resonance Raman spectra of SWNTs obtained from ACCVD with reduced Co amount on the quartz substrate.

catalytically active species in ACCVD, changing the amount of Mo can change the stabilization of Co influenced on the SWNT diameter. As shown in Figure 4-11, changing the amount of Mo from a standard recipe resulted in different stabilization of Co, which was demonstrated by changing the SWNTs diameter. An obvious blue shift of the E_{11} peak in the optical absorbance indicates that a smaller mean diameter of SWNT is obtained, even though optical absorbance does not show the real diameter distribution. The mean SWNT diameter was reduced from 2.5 nm to 1.4 nm by enhancing the amount of Mo from 0.5 times (0.005 %wt) to 5 times (0.05 %wt) for the standard recipe. This also indicates that changing in SWNT diameter is very sensitive to the difference of Mo amount. This is consistent with the results form Ref. [31], claiming that Mo forms an oxide with strong interaction with Co, and stabilize Co at high temperature [31]. In addition, changing large amount of Co recipes also influence the diameter change of SWNT. This result was also confirmed by Raman spectra (Figure 4-12). The intensity of small-diameter RBM peak around 250 cm^{-1} was increased with lower concentration of Co. It was also noticed that the Breit-Wigner-Fano (BWF) features in the G-band region shows the increasing of the population of small-diameter metallic SWNTs in the case of lower concentration of Co catalyst. Changing the Co recipe is, however, still not as sensitive as changing the Mo recipe.

4.10 A new noble catalyst for ACCVD process

In this section, I used Rh to stabilize Co catalyst and reduce the diameter of SWNTs synthesized on both Si substrates and zeolite particles. Figure 4-13 shows resonance Raman spectra obtained with different excitation wavelengths (488, 514 and 633 nm) for SWNTs grown from Co/Rh and Co/Mo bimetal catalysts. The shift in spectra weight toward higher energy indicates the SWNT diameters are smaller in the Co/Rh bimetal system. This can be explained by a strong interaction between Rh and Co, which keeps the nanoparticle diameter small and has been shown to result in increased magnetization [69] for Co/Rh. The yield of SWNTs, however, was much lower than from Co/Mo because the growth-stage energetics is more favorable [70] for Mo than for Rh.

In an attempt to improve both the yield and diameter selectivity of the Co/Rh catalysts, USY-zeolite was used as a supporting material. Figure 4-14 shows thermo-gravimetric analysis (TGA) data from as-grown SWNTs from different bimetals catalytic powders (Co-Rh, Co-Mo and Co-Fe). The growth temperature and pressure were fixed at 800˚C and

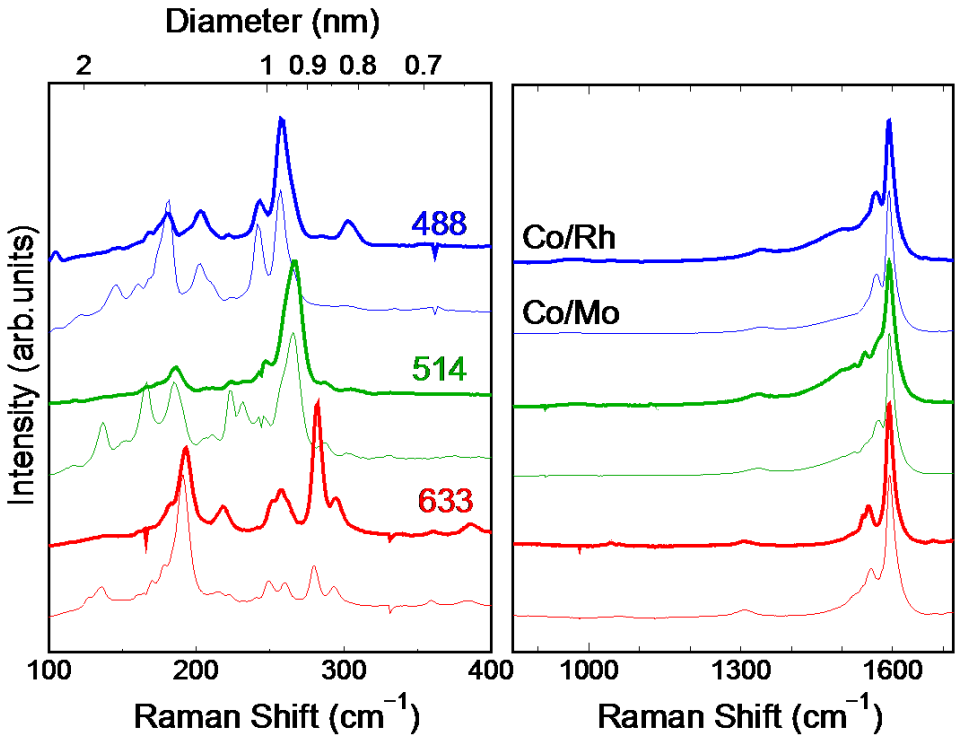

Figure 4-13 Resonance Raman spectra of SWNTs grown from the Co/Rh binary system (thick solid line) compared with those grown from the Co/Mo binary system (thin solid line). Excitation laser wavelengths (in nm) are indicated next to the spectra, and the colors correspond approximately to the color of the excitation laser.

10 torr (1.3 kPa) for 10 min. The burning temperature of SWNTs grown from Co-Rh and Co-Fe was found to be around 500°C. This agrees with our previous report [19], which corresponds to the burning point of SWNTs. At the first stage, TGA and DTG curve show that the metal particles were oxidized earlier at temperatures around 200°C, where the decomposition of Co-Mo metal catalysts is the highest, followed by Co-Rh and CoFe metal particles, respectively. There is a broad shoulder, which indicates burning of some kind of carbon species (amorphous carbon), that was observed around 300°C for Co-Rh and CoFe case and 250°C for Co-Mo case. In addition, there is another peak observed around 350°C in the case of Co-Rh and 400°C for Co-Mo. It can be noted that a temperature of 400°C in the case of Co-Mo should result from burning of SWNTs, because no other peaks were observed at temperatures higher than 500°C. As for the burning point around 300°C for Co-Rh case, we consider two possible explanations: this burning point might be from decomposition of other carbon species (amorphous carbon), or it might be from earlier burned SWNT itself, since the strong interaction between catalysts and SWNTs, and also oxidation peaks of metal catalysts (300°C) are also close to 350°C. Furthermore, TGA

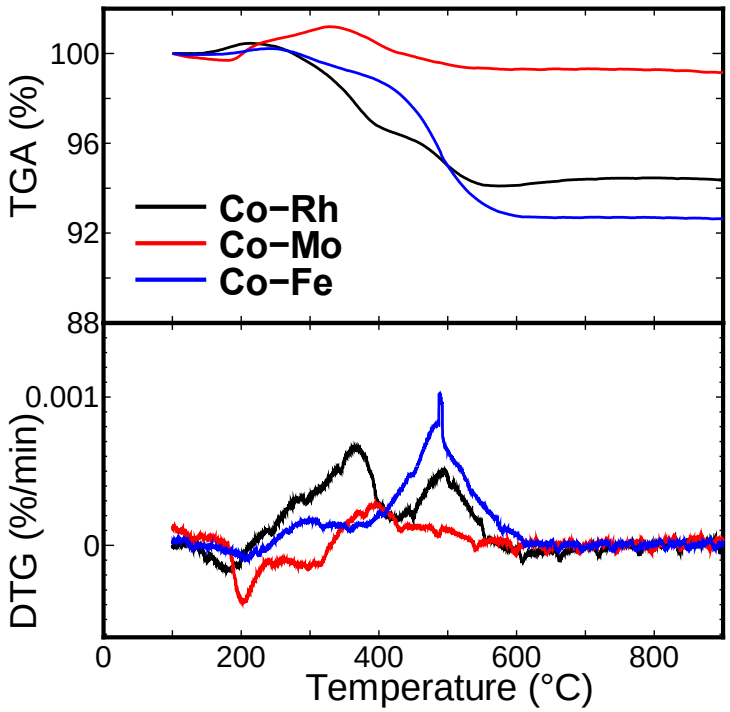

Figure 4-14 Thermo-gravimetric analysis (TGA) of SWNTs grown from different catalytic powders, shows the difference in the yield of SWNTs.

curve seems to slightly increase after a temperature of 600°C, this might be because some of catalysts remain on zeolite and were oxidized at higher temperature, gaining slightly higher mass, and this also can support the second possibility.

As for the yield of SWNT, the Co-Fe binary catalysts can still produce higher yield than others, even though the SWNT diameter is similar to the case of Co-Rh (see Figure 4-15). However, it was very surprising that Co-Mo catalysts on zeolite produced the lowest in yield. Figure 4-15 shows resonance Raman spectra of as-grown SWNTs synthesized from different catalytic powders measured using three different excitation wavelengths (488, 514 and 633 nm), which indicate that SWNTs grown from Co-Mo binary catalysts have larger diameters, whereas Co-Rh and Co-Fe catalyst systems produce smaller SWNTs. In addition, the similarity in diameters of SWNTs synthesized from Co-Fe and Co-Rh catalytic powder was also confirmed from UV-vis-NIR absorbance spectra (Figure 4-16). It is more consistent with results from resonance Raman spectrum that their diameter ranges are close to each other, but absorbance peaks of SWNTs grown from Co-Mo catalytic powder were shifted to the larger diameter. Figure 4-17a shows a photoluminescence excitation (PLE) map of suspended SWNTs grown from various catalyst powders and HiPco sample, which are the same as those used for absorbance

measurement. The fluorescence emission wavelength range was recorded from 900 to 1400 nm, while the excitation wavelength was scanned from 500 to 850 nm in 5 nm steps. Each peak in the PLE map corresponds to emission of the first electrical band gap (E_{11}) of semiconducting SWNT, first excited to the second electrical band gap (E_{22}). It shows that Co-Fe and Co-Rh binary catalysts can produce SWNTs that are similar in diameter, yet both of which are smaller than HiPco SWNTs. The SWNTs grown from these catalysts are dominant in (7, 5) and (7, 6) nanotubes, but SWNTs grown from Co-Rh can produce a bit more of (6, 5) nanotubes, which is identified from the intensity. The tendency for Co/Mo catalyst to produce SWNTs with a larger average diameter is in agreement with optical and resonance Raman spectra, however PLE indicates that SWNTs synthesized from Co-Mo catalyst on zeolite have a narrower diameter distribution than others, including HiPco. The chirality indices of SWNTs in both the Co-Mo and HiPco cases are dominant in (7,6) and (8,6). In addition, the diameter distribution of SWNT in the case of Co-Rh seems to be narrower than the case of Co-Fe and HiPco. Furthermore, the presence of SWNTs in all of samples was confirmed by TEM (Figure 4-17b) which is consistent with the TGA and DTG curve. Although carbon nanotubes were wrapped by surfactant, there are fully with SWNTs in all of samples with average diameter about 1 nm in the case of Co-Rh and Co-Fe, and 1.4 for Co-Mo case. The mean diameter of SWNTs synthesized using this binary system is similar to that from ACCVD sample [19].

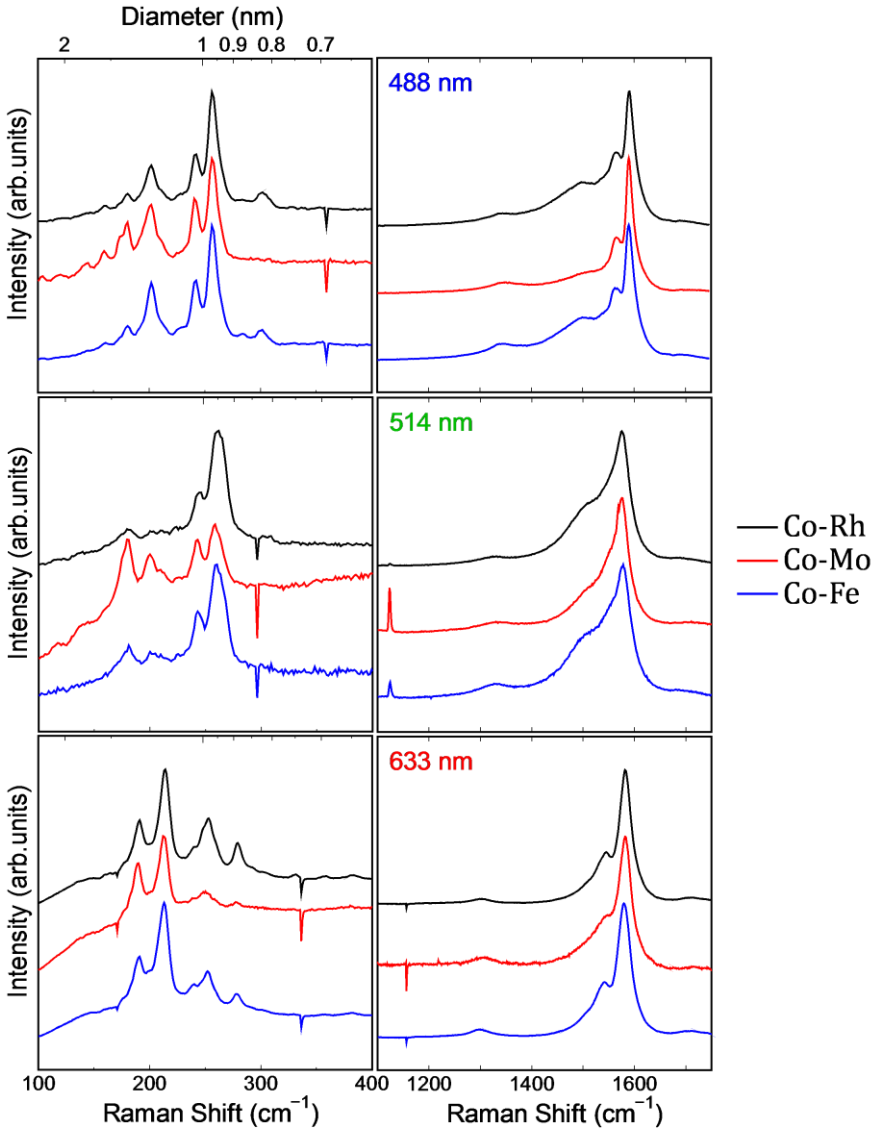

Figure 4-15 Raman spectra of SWNTs grown from different catalytic powders with different excitation energies.

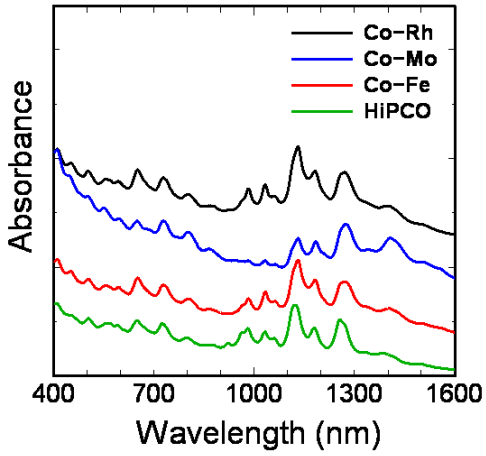

Figure 4-16 Absorbance spectra of SWNTs grown from different catalytic powders.

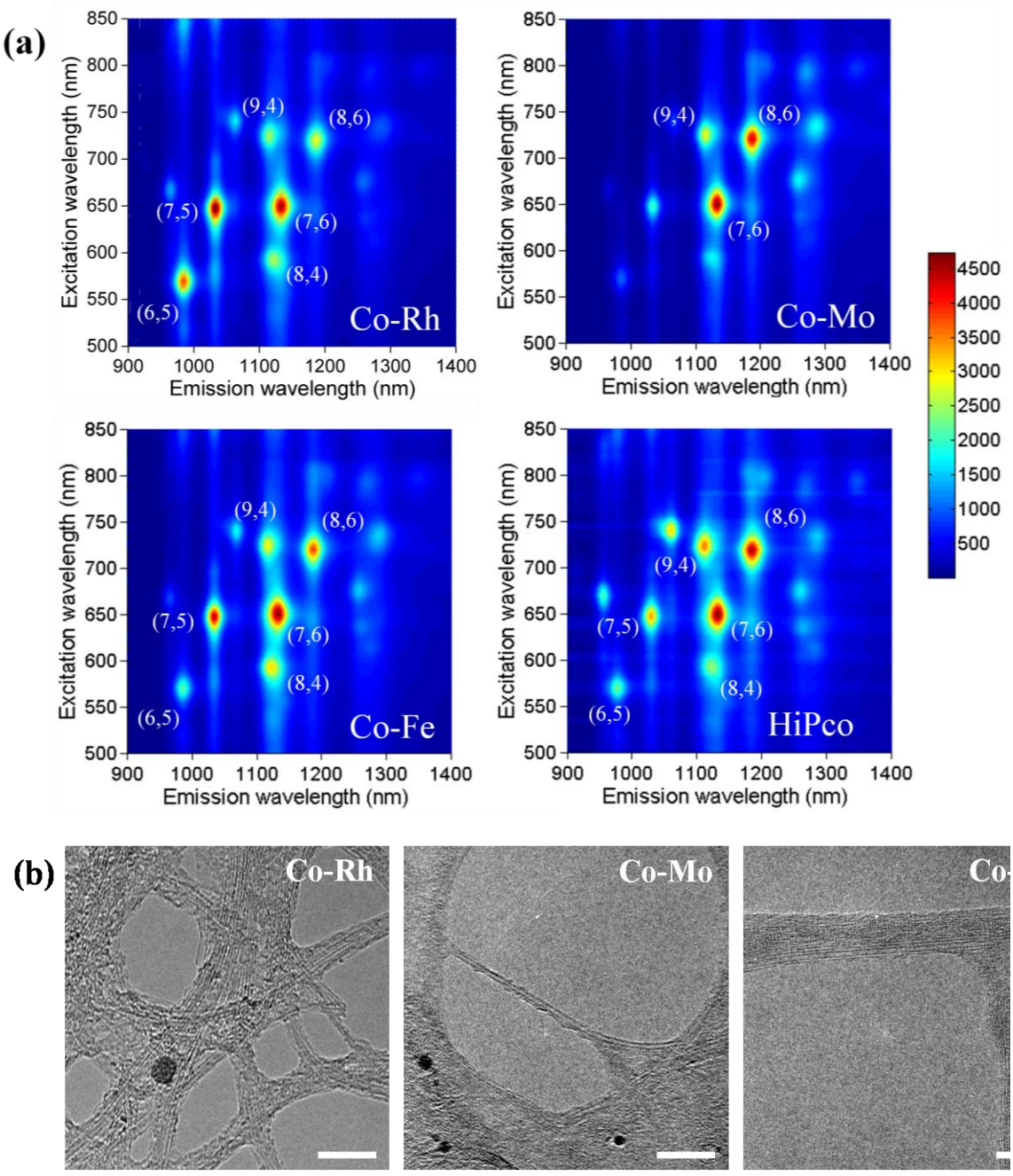

Figure 4-17 (a) Photoluminescence excitation (PLE) maps of SWNT sample grown from three different catalysts, compared with that from HiPco SWNTs, and (b) TEM images of SWNTs grown from different catalytic powder (scale bar shown 20 nm).

Chapter 5

Summary

In this research, several methods were proposed to reduce the diameter of SWNT, and were employed to systematically investigate diameter-controlled synthesis of single-walled carbon nanotubes (SWNTs). The influence of various parameters, such as ambient gas, substrate, catalyst pretreatment, catalyst recipe and the catalyst itself, was studied from large scale parameters to small scale parameters through the alcohol catalytic chemical vapor deposition (ACCVD) method. The results from resonance Raman spectroscopy, optical spectroscopy, and photoluminescence excitation spectroscopy (PLE) suggest that there are no influences of incurred by different ambient gases (Ar, He and N_2) on SWNT diameter under the conditions investigated.

Since the interaction with the catalyst affects their coarsening and surface diffusion of the supporting material, catalyst support surface as aluminum oxide (Al_2O_3) can be used to reduce the average SWNT diameter while maintaining the vertically aligned morphology.

Furthermore, the agglomeration of the catalysts is also sensitive to the reduction process. As a result, the average diameter of SWNTs was found to be dependent on reduction temperature and time. A trend toward smaller diameter for catalyst reduction can be achieved at lower temperatures. The morphology of SWNTs also changed from vertically aligned to random aligned for catalyst reduction at temperatures below 500˚C. The diameter of the SWNTs was also found to be slightly bigger after reduction for an extended period of time (more than 30 min) at a fixed temperature of 700˚C. The small diameter SWNTs on flat surface

can be also gained from adding water during annealing of catalysts before ACCVD process.

Catalyst agglomeration is also dependent upon the ratio of metals in the binary catalyst recipe. Thus, the average diameter of VA-SWNTs can be also reduced down to 1.4 nm by changing the catalyst recipe. In addition, small diameter SWNTs can be achieved by combining of Rhodium and cobalt (Rh-Co), with diameters as small as SWNTs produced from Co-Fe and HiPco samples.

Bibliography

[1] H. W. Kroto, J. R. Heath, S. C. O'Brien, R. F. Curl, R. E. Smalley, *Nature* 318 (1985) 162.

[2] S. Iijima, T. Ichihashi, *Nature* 363 (1993) 603.

[3] A. Thess, R. Lee, P. Nikolaev, H. Dai, P. Petit, J. Robert, C. Xu, Y. H. Lee, S. G. Kim, A. G. Rinzler, D. T. Colbert, G. E. Scuseria, D. Tománek, J. E. Fischer, R. E. Smalley, *Science* 273 (1996) 483.

[4] C. Journet, W. K. Maser, P. Bernier, A. Loiseau, M. L. de la Chapelle, S. Lefrant, P. Deniard, R. Lee, J. E. Fisher, *Nature* 388 (1997) 756.

[5] H. Dai, A. G. Rinzler, P. Nikolaev, A. Thess, D. T. Colbert, R. E. Smalley, *Chem. Phys. Lett.* 260 (1996) 471.

[6] B. C. Satishkumar, A. Govindaraj, R. Sen, C. N. R. Rao, *Chem. Phys. Lett.* 293 (1998) 47.

[7] H. M. Cheng, F. Li, G. Su, H. Y. Pan, L. L. He, X. Sun, M. S. Dresselhaus, *Appl. Phys. Lett.* 72 (1998) 3282.

[8] S. Maruyama, R. Kojima, Y. Miyauchi, S. Chiashi, M. Kohno, *Chem. Phys. Lett.* 360 (2002) 229.

[9] R. Saito, G. Dresselhaus, M. S. Dresselhaus, *Physical Properties of Carbon Nanotubes*, Imperial College Press, London, 1998.

[10] L. Couture-Mathieu, J. P. Mathieu, *Acta Cryst.* 5 (1952) 571.

[11] M. S. Dresselhaus, P. C. Eklund, *Adv. in Phys.* 49 (2000) 705.

[12] M. A. Pimenta, A. Marucci, S. Empedocles, M. Bawendi, E. B. Hanlon, A. M. Rao, P. C. Eklund, R. E. Smalley, G. Dresselhaus, M. S. Dresselhaus, *Phys. Rev. B* 58 (1998) R16016.

[13] S. D. M. Brown, A. Jorio, P. Corio, M. S. Dresselhaus, G. Dresselhaus, R. Saito, K. Kneipp, *Phys. Rev. B* 63 (2001) 155414.

[14] Y. Kawashima, G. Katagiri, *Phys. Rev. B* 59 (1999) 62.

[15] Y. Murakami, S. Chiashi, E. Einarsson, S. Maruyama, *Phys. Rev. B* 71 (2005) 085403.

[16] R. Saito, A. Gruneis, G. G. Samsonidze, G. Dresselhaus, M. S. Dresselhaus, A. Jorio, L. G. Cancado, M. A. Pimenta, A. G. Souza, *Applied Physics a-Materials Science & Processing* 78 (2004) 1099.

[17] S. M. Bachilo, M. S. Strano, C. Kittrell, R. H. Hauge, R. E. Smalley, R. B. Weisman, *Science* 298 (2002) 2361.

[18] J. P. C. Trigueiro, G. G. Silva, R. L. Lavall, C. A. Furtado, S. Oliveira, A. S. Ferlauto, R. G. Lacerda, L. O. Ladeira, J. W. Liu, R. L. Frost, G. A. George, *J. Nanosci. Nanotech.* 7 (2007) 3477.

[19] Y. Murakami, Y. Miyauchi, S. Chiashi, S. Maruyama, *Chem. Phys. Lett.* 374 (2003) 53.

[20] A. C. Dillon, T. Gennett, K. M. Jones, J. L. Alleman, P. A. Parilla, M. J. Heben, *Adv. Mater.* 11 (1999) 1354.

[21] P. Nikolaev, M. J. Bronikowski, R. K. Bradley, F. Rohmund, D. T. Colbert, K. A. Smith, R. E. Smalley, *Chem. Phys. Lett.* 313 (1999) 91.

[22] Y. Murakami, S. Chiashi, Y. Miyauchi, M. H. Hu, M. Ogura, T. Okubo, S. Maruyama, *Chem. Phys. Lett.* 385 (2004) 298.

[23] R. Xiang, E. Einarsson, J. Okawa, T. Thurakitseree, Y. Murakami, J. Shiomi, Y. Ohno, S. Maruyama, *J. Nanosci. Nanotechnol.* 10 (2010) 3901.

[24] S. Han, X. L. Liu, C. W. Zhou, *J. Am. Chem. Soc.* 127 (2005) 5294.

[25] A. Ismach, L. Segev, E. Wachtel, E. Joselevich, *Angew. Chem.-Int. Edit.* 43 (2004) 6140.

[26] C. Kocabas, S. H. Hur, A. Gaur, M. A. Meitl, M. Shim, J. A. Rogers, *Small* 1 (2005) 1110.

[27] C. Kocabas, M. Shim, J. A. Rogers, *J. Am. Chem. Soc.* 128 (2006) 4540.

[28] Y. Shibuta, S. Maruyama, *Chem. Phys. Lett.* 382 (2003) 381.

[29] A. Jorio, G. Dresselhaus, M. S. Dresselhaus, *Carbon nanotubes: advanced topics in the synthesis, structure, properties and applications*, Springer, Heidelberg, 2008.

[30] Y. Murakami, Y. Miyauchi, S. Chiashi, S. Maruyama, *Chem. Phys. Lett.* 377 (2003) 49.

[31] M. H. Hu, Y. Murakami, M. Ogura, S. Maruyama, T. Okubo, *J. Catal.* 225 (2004) 230.

[32] K. Mukhopadhyay, A. Koshio, N. Tanaka, H. Shinohara, *Jpn. J. Appl. Phys.* 37 (1998) L1257.

[33] K. Mukhopadhyay, A. Koshio, T. Sugai, N. Tanaka, H. Shinohara, Z. Konya, J. B. Nagy, *Chem. Phys. Lett.* 303 (1999) 117.

[34] Y. Homma, Y. Kobayashi, T. Ogino, D. Takagi, R. Ito, Y. J. Jung, P. M. Ajayan, *J. Phys. Chem. B* 107 (2003) 12161.

[35] G. F. Zhong, T. Iwasaki, K. Honda, Y. Furukawa, I. Ohdomari, H. Kawarada, *Chem. Vapor. Depos.* 11 (2005) 127.

[36] G. Y. Zhang, D. Mann, L. Zhang, A. Javey, Y. M. Li, E. Yenilmez, Q. Wang, J. P. McVittie, Y. Nishi, J. Gibbons, H. J. Dai, *Proc. Natl. Acad. Sci. U.S.A.* 102 (2005) 16141.

[37] Y. Q. Xu, E. Flor, M. J. Kim, B. Hamadani, H. Schmidt, R. E. Smalley, R. H. Hauge, *J. Am. Chem. Soc.* 128 (2006) 6560.

[38] G. Eres, A. A. Kinkhabwala, H. T. Cui, D. B. Geohegan, A. A. Puretzky, D. H. Lowndes, *J. Phys. Chem. B* 109 (2005) 16684.

[39] S. Noda, K. Hasegawa, H. Sugime, K. Kakehi, Z. Y. Zhang, S. Maruyama, Y. Yamaguchi, *Jap. J. Appl. Phys. Part 2-Letters & Express Letters* 46 (2007) L399.

[40] L. Zhang, Y. Q. Tan, D. E. Resasco, *Chem. Phys. Lett.* 422 (2006) 198.

[41] K. Hata, D. N. Futaba, K. Mizuno, T. Namai, M. Yumura, S. Iijima, *Science* 306 (2004) 1362.

[42] Y. Murakami, E. Einarsson, T. Edamura, S. Maruyama, *Carbon* 43 (2005) 2664.

[43] Y. Zhang, A. Chang, J. Cao, Q. Wang, W. Kim, Y. Li, N. Morris, E. Yenilmez, J. Kong, H. Dai, *Appl. Phys. Lett.* **79** (2001) 3155.

[44] E. Joselevich, C. M. Lieber, *Nano Lett.* **2** (2002) 1137.

[45] M. Maeda, C. K. Hyon, T. Kamimura, A. Kojima, K. Sakamoto, K. Matsumoto, *Jap. J. Appl. Phys.* **44** (2005) 1585.

[46] S. Huang, X. Cai, C. Du, J. Liu, *J. Phys. Chem. B* **107** (2003) 13251.

[47] L. X. Zheng, M. J. O'Connell, S. K. Doorn, X. Z. Liao, Y. H. Zhao, E. A. Akhadov, M. A. Hoffbauer, B. J. Roop, Q. X. Jia, R. C. Dye, D. E. Peterson, S. M. Huang, J. Liu, Y. T. Zhu, *Nat. Mater.* **3** (2004) 673.

[48] V. Derycke, R. Martel, M. Radosavljević, F. M. Ross, Ph. Avouris, *Nano Lett.* **2** (2002) 1043.

[49] A. Ismach, D. Kantorovich, E. Joselevich, *J. Am. Chem. Soc.* **127** (2005) 11554.

[50] D. Yuan, L. Ding, H. Chu, Y. Feng, T. P. McNicholas, J. Liu, *Nano Lett.* 8 (2008) 2576.

[51] W. Zhou, L. Ding, S. Yang, J. Liu, *J. Am. Chem. Soc.* 132 (2010) 336.

[52] D. Phokharatkul, Y. Ohno, H. Nakano, S. Kishimoto, T. Mizutani, *Appl. Phys. Lett.* 93 (2008) 053112.

[53] Y. Murakami, S. Chiashi, Y. Miyauchi, M. Hu, M. Ogura, T. Okubo, S. Maruyama, *Chem. Phys. Lett.* 385 (2004) 298.

[54] R. H. Baughman, A. A. Zakhidov, W. A. de Heer, *Science* 297 (2002) 787.

[55] H. Liu, T. Chokan, D. Takagi, H. Ohno, S. Chiashi, Y. Homma, *Jap. J. Appl. Phys.* 47 (2008) 1966.

[56] A. R. Harutyunyan, G. Chen, T. M. Paronyan, E. M. Pigos, O. A. Kuznetsov, K. Hewaparakrama, S. M. Kim, D. Zakharov, E. A. Stach, G. U. Sumanasekera, *Science* 326 (2009) 116.

[57] C. M. Fu, A. M. Schaffer, *Ind. Eng. Chem. Prod. Res. Dev.* 24 (1985) 68.

[58] Y. Murakami, S. Chiashi, Y. Miyauchi, S. Maruyama, *Jap. J. Appl. Phys.* 43 (2004) 1221.

[59] B. Wang, Y. Yang, L. J. Li, Y. Chen, *J. Mater. Sci.* 44 (2009) 3285.

[60] H. Ago, S. Imamura, T. Okazaki, T. Saito, M. Yumura, M. Tsuji, *J. Phys. Chem. B* 109 (2005) 10035.

[61] G. Lolli, L. Zhang, L. Balzano, N. Sakulchaicharoen, Y. Tan, D. E. Resasco, *J. Phys. Chem. B* 110 (2006) 2108.

[62] E. Einarsson, Y. Murakami, M. Kadowaki, , H. M. Duong, M. Inoue, S. Maruyama, *Therm. Sci. Eng.* 14 (2006) 47.

[63] T. Saito, S. Ohmori. B. Sukla, M. Yumura, S. Iijima, *Appl. Phys. Express* 2 (2009) 095006.

[64] D. N. Futaba, K. Hata, T. Namai, T. Yamada, K. Mizuno, Y. Hayamizu, M. Yumura, S. Iijima, *J. Phys. Chem. B* 110 (2006) 8035.

[65] P. B. Amama, C. L. Pint, L. McJilton, S. M. Kim, E. A. Stach, P. T. Murray, R. H. Hauge, B. Maruyama, *Nano Lett.* 9 (2009) 44.

[66] G. L. Bezemer, T. J. Remans, A. P. van Bavel, A. I. Dugulan, *J. Am. Chem. Soc.* 132 (2010) 8540.

[67] R. Hakkarainen, T. Salmi, *Appl. Catalyst A* 99 (1993) 195.

[68] S. Helveg, C. L. Cartes, J. Sehested, P. L. Hansen, B. S. Clausen, J. R. R. Nielsen, F. A. Pedersen, J. K. Norskov, *Nature* 427 (2004) 426.

[69] J.W.A. Robinson, Z.H. Barber, M.G. Blamire, *Appl. Phys. Lett.* 95 (2009) 192509.

[70] W. Q. Deng, X. Xu, W. A. Goddard, *Nano Lett.* 4 (2004) 2331.

Acknowledgement

First and foremost, I am very grateful to the Office of the Higher Education Commission, which always supported me during my master course. In these two years of master course, I am also very grateful and appreciative of my advisor, Professor Shigeo Maruyama, who gave me the precious opportunity to study in his laboratory and at The University of Tokyo, even though my English was very bad when I first came to Japan. I have gradually learned and improved English and also developed my Japanese. I thank him for many things that I cannot enumerate here but mostly for his advice, understanding and patience. I would also like to thank the person, who has always helped me, Erik. He has advised me when I had problems, and particularly for the help he gave me in revising many of my papers.

This thesis would not have been possible without the kindness from Xiang Rong, who has taught me how to do experiments and real research, synthesize SWNTs, operate machines and obtain analysis, including providing new ideas. I also thank other members in Maruyama-Shiomi laboratory, Shinya Aikawa for the assistance on TEM observation and catalyst patterning, Shohei Chiashi for the assistance on Raman measurement, Pei Zhao, Hiroto Okabe and Taiki Inoue.

Finally, I would like to thank my family for their encouragement and am only too indebted to my mother, who gave me this chance for studying in the Master course by offering the funds necessary for me at the time I was undergraduate student.

以上

修士論文

単層カーボンナノチューブの直径制御 CVD 合成

Diameter controlled CVD growth of single-walled carbon nanotubes

1 - 58 ページ 完

平成 22 年 8 月 20 日提出

Submitted on Aug. 20, 2010

指導教員 丸山茂夫教授

Supervised by Professor Shigeo Maruyama

Theerapol THURAKITSEREE

37-085938 トゥラキットセーリー ティーラポン